

CERN-PH-EP-2015-030
February 12, 2015

Rapidity and transverse-momentum dependence of the inclusive J/ψ nuclear modification factor in p-Pb collisions at $\sqrt{s_{NN}} = 5.02$ TeV

ALICE Collaboration

Abstract

We have studied the transverse-momentum (p_T) dependence of the inclusive J/ψ production in p-Pb collisions at $\sqrt{s_{NN}} = 5.02$ TeV, in three center-of-mass rapidity (y_{cms}) regions, down to zero p_T . Results in the forward and backward rapidity ranges ($2.03 < y_{cms} < 3.53$ and $-4.46 < y_{cms} < -2.96$) are obtained by studying the J/ψ decay to $\mu^+\mu^-$, while the mid-rapidity region ($-1.37 < y_{cms} < 0.43$) is investigated by measuring the e^+e^- decay channel. The p_T dependence of the J/ψ production cross section and nuclear modification factor are presented for each of the rapidity intervals, as well as the J/ψ mean p_T values. Forward and mid-rapidity results show a suppression of the J/ψ yield, with respect to pp collisions, which decreases with increasing p_T . At backward rapidity no significant J/ψ suppression is observed. Theoretical models including a combination of cold nuclear matter effects such as shadowing and partonic energy loss, are in fair agreement with the data, except at forward rapidity and low transverse momentum. The implications of the p-Pb results for the evaluation of cold nuclear matter effects on J/ψ production in Pb-Pb collisions are also discussed.

arXiv:1503.07179v1 [nucl-ex] 24 Mar 2015

The suppression of charmonia, bound states of c and \bar{c} quarks, and in particular of the J/ψ state, has long been proposed as a signature for the formation of a plasma of quarks and gluons (QGP) [1] in ultrarelativistic nucleus-nucleus collisions. However, it was soon realized that charmonium production can also be modified by nuclear effects not necessarily related to QGP formation [2]. These so-called cold nuclear matter (CNM) effects can be investigated by studying charmonium production in proton-nucleus (p-A) collisions as confirmed by the analysis of results obtained by several fixed-target (SPS [3, 4], HERA [5] and Tevatron [6]) and collider (RHIC [7] and LHC [8, 9]) experiments.

Theoretical models have studied the production of charmonium in p-A collisions and the effects of the surrounding cold nuclear medium by introducing various mechanisms which include nuclear shadowing, gluon saturation, energy loss and nuclear absorption. Models [10–12] inspired by Quantum ChromoDynamics (QCD) describe charmonium production as a two-step process, with the $c\bar{c}$ pair created in a hard parton scattering, followed by its evolution into a bound state with specific quantum numbers. The pair creation is sensitive to the Parton Distribution Functions (PDFs) in both colliding partners and, at high energy, occurs mainly via gluon fusion. Although PDFs are known to be modified in a nuclear environment, information on the dependence of such modifications on the fraction x (Bjorken- x) of the nucleon momentum carried by the gluons and on the four-momentum squared Q^2 transferred in the scattering is still limited [13–15]. Charmonium production measurements can therefore provide insight into the so-called nuclear shadowing, i.e., on how the nucleon gluon PDFs are modified in a nucleus.

Modifications of the initial state of the nucleus are also addressed by approaches assuming that at sufficiently high energies, when the quark pair is produced from a dense gluon system carrying small x -values in the nuclear target, a coherent effect known as gluon saturation sets in. Such an effect can be described by the Color Glass Condensate (CGC) effective theory, which is characterized by a saturation momentum scale (Q_s^2). When combined with a specific quarkonium production model [16, 17], it is able to provide predictions for charmonium production in p-A collisions. In the context of shadowing and CGC models, a measurement of the charmonium yield as a function of transverse momentum (p_T) and rapidity (y) is important as it gives access to specific ranges of values of the gluon x and/or Q^2 .

In addition to these purely initial state effects, both the incoming partons and the $c\bar{c}$ pair propagating through the nucleus may lose energy by gluon radiation at the various stages of the charmonium formation process [18]. The interference of gluons radiated before and after the hard production vertex can lead to coherent energy loss effects, expected to induce a modification of the charmonium kinematic distributions [19].

Finally, while travelling through nuclear matter, the evolving $c\bar{c}$ pair or, if crossing times are sufficiently large, the fully formed resonance, may break-up into open charm meson pairs. Although this mechanism, known as nuclear absorption, plays an important role at lower collision energies [4], at the LHC the contribution of this effect to the production cross section is expected to be small, due to the very short crossing time of the pair through the nuclear environment.

Understanding the role of the cold nuclear matter effects outlined above is essential to further our knowledge of various aspects of the physics of strong interactions, and it is crucial for the interpretation of the results on charmonium production in heavy-ion collisions, where the formation of a QGP is expected. In such a hot and dense deconfined medium the color screening mechanism (the QCD analogue of the Debye screening in QED) can prevent the formation of the heavy-quark bound states, leading to a suppression of quarkonium production [1]. In addition, at LHC energies, the large charm quark density may lead to a (re)generation of charmonium by (re)combination of charm quarks [20, 21] in the QGP phase and/or when the system cools down and the formation of hadrons occurs. This effect enhances charmonium production and is expected to be particularly sizeable at low p_T . In heavy-ion collisions, a superposition of hot and cold nuclear matter effects is expected, and a quantitative evaluation of the latter is an important prerequisite for a detailed understanding of the former. At lower energy, both at SPS [22–24] and RHIC [25, 26], a suppression of J/ψ production, in addition to the CNM effects estimated from p-A(d-A) collisions, was indeed observed.

A suppression of J/ψ production has been measured in Pb–Pb collisions at the LHC [27–31]. It was quantified via the nuclear modification factor, i.e., the ratio of the Pb–Pb yields with respect to those measured in pp at the same energy, scaled by the number of binary nucleon-nucleon collisions. The suppression has been found to be stronger at forward rapidity and at high p_T [30,31], in agreement with expectations from (re)combination models. Similar to the lower energy experiments, accurate measurements in p–A collisions are needed to quantitatively assess the contribution of hot and cold nuclear matter effects in Pb–Pb.

The first measurements of inclusive J/ψ production in p–Pb collisions at the LHC at $\sqrt{s_{NN}} = 5.02$ TeV [8,9] have shown a sizeable suppression, with respect to binary-scaled pp collisions, at forward rapidity (p-going side) and no suppression at backward rapidity (Pb-going side). The nuclear modification factors are in fair agreement with models based on nuclear shadowing [32,33]. Calculations including a contribution from coherent energy loss [19] also reproduce the data. Corresponding measurements for the less strongly bound $\psi(2S)$ charmonium state are presented in [34]. In addition, an extrapolation to Pb–Pb collisions of the J/ψ suppression measured in p–Pb showed that the effects observed in Pb–Pb cannot be ascribed only to CNM [8].

In this situation, a study of the transverse-momentum dependence of J/ψ production at LHC energies for various rapidity regions is particularly interesting in order to: (i) reach a deeper understanding and better quantify the complicated interplay of CNM effects, which are expected to exhibit a well-defined kinematical dependence [33,35,36]; (ii) determine if the differential features of the Pb–Pb results that suggest the presence of (re)combination effects are still present when the contribution of CNM is considered.

In this paper, we present ALICE results on the transverse-momentum dependence of the inclusive J/ψ production in p–Pb collisions at $\sqrt{s_{NN}} = 5.02$ TeV, measured in three center-of-mass rapidity (y_{cms}) ranges: backward ($-4.46 < y_{cms} < -2.96$), mid- ($-1.37 < y_{cms} < 0.43$) and forward ($2.03 < y_{cms} < 3.53$). The data are from the 2013 LHC p–Pb run.

At mid-rapidity, J/ψ are reconstructed in the e^+e^- decay channel with the ALICE central barrel detectors, covering the pseudorapidity range $|\eta_{lab}| < 0.9$. For the backward and forward rapidity analysis, J/ψ are detected, through their $\mu^+\mu^-$ decay channel in the muon spectrometer, in the pseudorapidity range $-4 < \eta_{lab} < -2.5$.

Due to the energy asymmetry of the LHC beams ($E_p = 4$ TeV and $E_{Pb} = 1.58 \cdot A_{Pb}$ TeV, where $A_{Pb} = 208$ is the Pb atomic mass number), the nucleon-nucleon center-of-mass is shifted, with respect to the laboratory frame, by $\Delta y = 0.465$ in the direction of the proton beam. Since data were collected in two configurations, interchanging the direction of the proton and the Pb beams in the LHC, the muon spectrometer acceptance covers the forward and backward y_{cms} regions quoted above, where positive (negative) rapidities refer to the direction of the proton (Pb) beam. In the following, the notation p–Pb (Pb–p) will refer to the first (second) configuration.

For the dielectron analysis, the central barrel detectors used for the J/ψ reconstruction are the Inner Tracking System (ITS) [37] and the Time Projection Chamber (TPC) [38]. The ITS contains six cylindrical layers of silicon detectors, with the innermost layer at a radius of 3.9 cm with respect to the beam axis and the outermost layer at 43 cm. This detector is used for reconstructing the primary interaction vertex as well as vertices from different interactions and secondary vertices from decays of heavy-flavored particles. The TPC has a cylindrical geometry with an active volume that extends from 85 to 247 cm in the radial direction and 500 cm longitudinally. It is the main central barrel tracking detector and also provides particle identification via the measurement of the specific energy loss (dE/dx) in the detector gas.

The muon spectrometer [39] is the main detector used in the dimuon analysis. It consists of a 3 T·m dipole magnet, coupled with a tracking and a triggering system. Between the interaction point and the

muon spectrometer, a ten interaction-length (λ_I) front absorber filters out the hadrons produced in the interaction. Muon tracking is performed by means of five tracking stations, each one made of two planes of Cathode Pad Chambers. A $7.2 \lambda_I$ iron wall, which stops secondary hadrons escaping the front absorber and low momentum muons, is placed after the tracking stations. It is followed by a muon trigger system, based on two stations equipped with Resistive Plate Chambers. A conical absorber made of tungsten, lead and steel protects the spectrometer against secondary particles produced by the interaction of large- η primary particles in the beam pipe. In the dimuon analysis, the determination of the interaction vertex is provided by the two innermost Si-pixel layers of the ITS (Silicon Pixel Detector, SPD).

For both analyses, timing information from the Zero Degree Calorimeters [40], placed symmetrically at 112.5 m with respect to the interaction point, is used to remove de-bunched proton-lead collisions. Furthermore, two scintillator hodoscopes (VZERO) [41], with pseudorapidity coverage $2.8 < \eta_{\text{lab}} < 5.1$ and $-3.7 < \eta_{\text{lab}} < -1.7$, are used to remove beam-induced background. More details on the ALICE apparatus can be found in [39].

A coincidence of signals in the two VZERO detectors provides the minimum bias (MB) trigger, which has a $> 99\%$ efficiency for selecting non single-diffractive p-Pb collisions [42]. While the dielectron analysis is based on MB-triggered events, the study of J/ψ in the $\mu^+\mu^-$ decay channel relies on a dimuon trigger which requires, in addition to the MB condition, the detection of two opposite-sign tracks in the trigger system. The dimuon trigger selects two muon candidates with transverse momenta $p_{T,\mu}$ larger than 0.5 GeV/c. The trigger threshold is not sharp, and the single muon trigger efficiency reaches its plateau value ($\sim 96\%$) at $p_{T,\mu} \sim 1.5$ GeV/c. The dielectron analysis was performed on a data sample corresponding to the p-Pb configuration, with an integrated luminosity $\mathcal{L}_{\text{int}} = 51.4 \pm 1.9 \mu\text{b}^{-1}$, while for the dimuon analysis the corresponding values are $5.01 \pm 0.19 \text{nb}^{-1}$ for p-Pb and $5.81 \pm 0.20 \text{nb}^{-1}$ for Pb-p (the quoted uncertainties are systematic) [43].

The dielectron analysis is based on 1.07×10^8 events, collected with a low MB interaction rate (~ 10 kHz), with a negligible amount of events having more than one interaction per bunch crossing (pile-up events). The interaction vertex is required to lie within ± 10 cm from the nominal collision point along the beam axis, in order to obtain a uniform acceptance of the central barrel detector system in the fiducial range $|\eta_{\text{lab}}| < 0.9$. Electron candidates are selected with criteria very similar to those used in previous analyses of pp collisions at $\sqrt{s} = 7$ TeV [44] and Pb-Pb collisions at $\sqrt{s_{\text{NN}}} = 2.76$ TeV [30]. To ensure a uniform tracking efficiency and particle identification resolution in the TPC, only tracks within $|\eta_{\text{lab}}| < 0.9$ are used. Electron identification is performed using the TPC, as shown in Fig. 1, by requiring the dE/dx signal to be compatible with the electron assumption within 3σ , where σ denotes the resolution of the dE/dx measurement. Furthermore, the TPC tracks that are compatible with the pion and proton assumptions within 3.5σ are rejected. A slightly looser rejection condition (3σ) is applied when considering tracks corresponding to dielectron candidates with $p_T > 5$ GeV/c in order to enhance the statistics. A cut on the transverse momentum ($p_{T,e} > 1.0$ GeV/c) is applied to remove combinatorial background from low-momentum electrons. The efficiency loss induced by this cut amounts to only $\sim 20\%$, due to the relatively large momentum of the J/ψ decay products. The electron candidates must have at least one hit in the innermost two layers of the ITS, thus rejecting a large fraction of background electrons from photon conversions. For dielectrons with $p_T < 3$ GeV/c the electron candidates are required to have a hit in the first layer, to further reduce background. The tracks are required to have at least 70 out of a maximum of 159 clusters in the TPC and a χ^2 normalized to the number of clusters attached to the track smaller than 4.

The J/ψ yields are obtained by counting the number of entries in the invariant mass range $2.92 < m_{e^+e^-} < 3.16$ GeV/c² after background subtraction. The J/ψ radiative decay channel and the energy loss of the electrons due to bremsstrahlung in the detector material produce a long tail towards low invariant masses. A fit using a Crystal Ball (CB) [45] function for the J/ψ signal gives compatible values in Monte-Carlo (MC) and data (~ 20 MeV/c² for the width of the Gaussian component of the CB). Taking into account

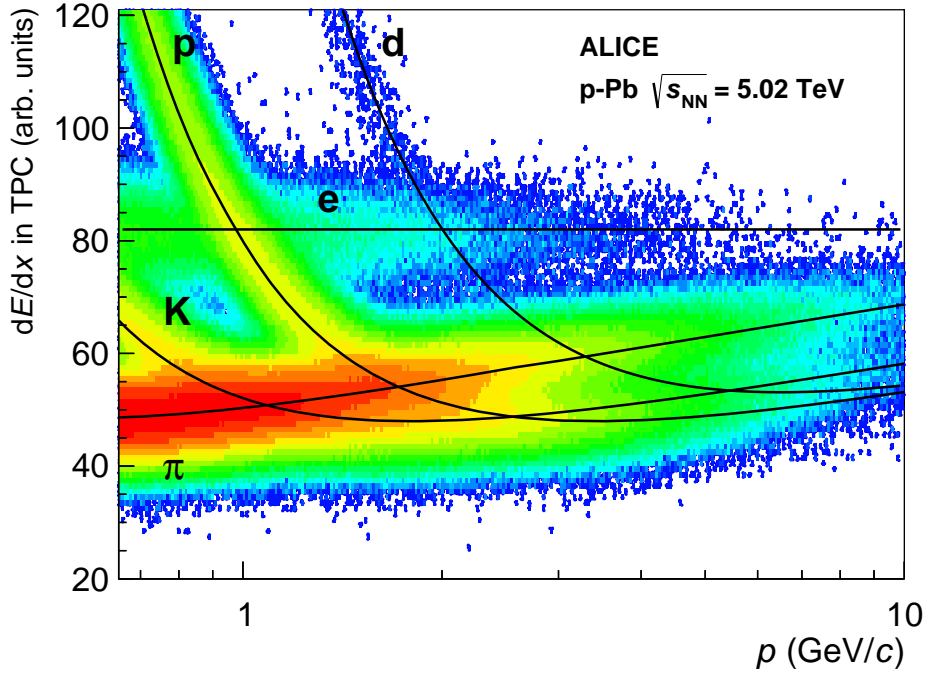


Fig. 1: Charged particle specific energy loss (dE/dx) as a function of momentum, as measured in the TPC in p-Pb collisions. The black lines are the corresponding Bethe-Bloch parametrizations for the various particle species.

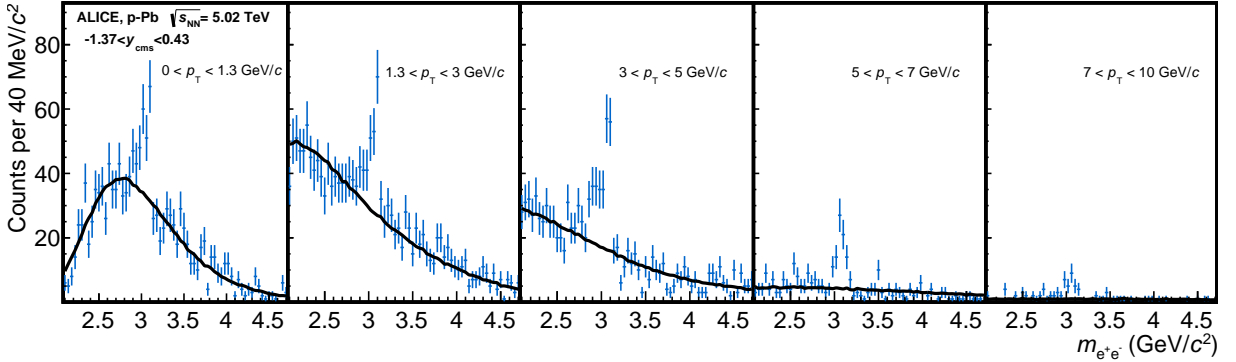


Fig. 2: Opposite-sign dielectron invariant mass spectra (blue symbols) for various p_T intervals, compared to the background (black curve) estimated through mixed events. The background is scaled to match the data in the mass ranges $2.0 < m_{e^+e^-} < 2.5 \text{ GeV}/c^2$ and $3.2 < m_{e^+e^-} < 3.7 \text{ GeV}/c^2$.

such a mass resolution and the presence of the bremsstrahlung tail, 67 – 73% of the signal, depending on p_T , falls within the counting window. The background shape is obtained from event mixing. Event mixing is performed by pairing leptons from different events having similar global characteristics such as the primary-vertex position and the track multiplicity (the result being quite insensitive to the rapidity range, either forward or central, chosen for the multiplicity measurements). The mixed-event background is then scaled to match the same-event opposite-sign distribution in the mass ranges $2.0 < m_{e^+e^-} < 2.5 \text{ GeV}/c^2$ and $3.2 < m_{e^+e^-} < 3.7 \text{ GeV}/c^2$ (the contribution of the bremsstrahlung tail in the former range and of the $\psi(2S)$ in the latter are negligible). Consistent results are found when the same-event like-sign distributions are used, instead of event mixing, to estimate the background. The systematic uncertainty on the signal extraction comes from the variation of the mass range where the normalization of the mixed-event background shape is performed and from the choice of the mass window where the

signal is counted. The signal extraction has been performed in five transverse-momentum bins, $p_T < 1.3$, $1.3 < p_T < 3$, $3 < p_T < 5$, $5 < p_T < 7$ and $7 < p_T < 10$ GeV/ c . The J/ψ counts in these bins vary from 25 to 132, with a significance, computed in the $2.92 < m_{e^+e^-} < 3.16$ GeV/ c^2 mass region, ranging from 4.6 to 8.7. An analysis of the p_T -integrated data sample, using the procedure detailed above, gives $465 \pm 37(\text{stat.}) \pm 16(\text{syst.})$ J/ψ signal counts. The systematic uncertainty on the signal extraction is largest at low p_T (10% for $p_T < 1.3$ GeV/ c and 12% for $1.3 < p_T < 3$ GeV/ c), due to a less favorable signal over background ratio, and decreases to ~ 5.5 – 8.4% in the other three p_T bins. Figure 2 shows the invariant mass distributions for the opposite-sign dielectrons compared with the mixed-event background for the different intervals of p_T .

The dimuon analysis is performed as detailed in [8], and is shortly summarized hereafter. Data were collected with the dimuon trigger, and the MB interaction rate (up to 200 kHz) was much higher than in the sample used for the dielectron analysis. This leads to a $\sim 2\%$ interaction pile-up probability. However, the probability of having more than one dimuon in the same bunch crossing satisfying the trigger condition is negligible. Muon candidate tracks are reconstructed in the tracking system by using the standard reconstruction algorithm [44]. The quality of the tracks is ensured by requiring the single muon pseudorapidity to be in the range $-4 < \eta_{\text{lab},\mu} < -2.5$, in order to remove particles at the edges of the muon spectrometer acceptance. In addition, a cut on the radial coordinate of the track at the end of the front absorber ($17.6 < R_{\text{abs}} < 89.5$ cm) is performed, ensuring rejection of muons crossing its high-density part, where energy loss and multiple scattering effects are more important. The tracks reconstructed in the tracking system that are not matched to a corresponding track in the triggering system are rejected [44]. Finally, the reconstructed dimuons are required to be in $2.03 < y_{\text{cms}} < 3.53$ ($-4.46 < y_{\text{cms}} < -2.96$) for the forward (backward) rapidity analysis. The number of J/ψ is extracted in transverse-momentum bins, in the range $p_T < 15$ GeV/ c , through fits to the invariant mass spectra of opposite-sign dimuons. The spectra are fitted with a superposition of background and resonance shapes. The background is described with a Gaussian function with a mass-dependent width or, alternatively, with an exponential function times a fourth-order polynomial function. For the J/ψ shape an extended Crystal Ball function, which accommodates a non-Gaussian tail both on the right and on the left side of the resonance peak, is adopted. Alternatively, a pseudo-Gaussian function [46] is used, corresponding to a Gaussian core around the J/ψ pole, and tails on the right and left side of it, parameterized by varying the width of the Gaussian as a function of the mass. The value of the J/ψ mass and its width (σ) at the pole position are free parameters of the fit. The mass coincides with the PDG value within less than 5 MeV/ c^2 and the width is ~ 70 MeV/ c^2 , slightly increasing with p_T , due to a small relative decrease in the tracking resolution for harder muons. Although the signal over background ratios, calculated for a $\pm 3\sigma$ interval around the resonance peak, are relatively large (ranging from 1.4 to ~ 6 moving from low to high p_T), the parameters of the tails of the J/ψ distributions cannot be reliably tuned on the data (in particular at large p_T , where statistics is limited), but are fixed, for each p_T bin, to the values extracted from fits to reconstructed samples from a signal-only MC generation. The contribution of the $\psi(2S)$ resonance is also included in the fitting procedure, even if its influence on the determination of the J/ψ yield is negligible. Finally, all the fits are performed in two different invariant mass ranges, either $2 < m_{\mu\mu} < 5$ GeV/ c^2 or $2.2 < m_{\mu\mu} < 4.5$ GeV/ c^2 . Examples of fits to the invariant mass spectra, in the p_T bins under study, are shown in Fig. 3.

For each p_T bin, the number of J/ψ is evaluated as the average of the integrals of the resonance functions obtained in the various fits. The RMS of the corresponding yield distributions (0.2 – 3%, depending on p_T) provides the systematic uncertainty on the signal extraction. Additional sets of tails, obtained from the MC, but referring to other y_{cms} and p_T phase space regions, have also been tested and the dependence of the extracted yields on the variation of the tails (2%) is included in the systematic uncertainty on the signal extraction. As a function of p_T , the number of J/ψ in the p–Pb (Pb–p) configuration ranges between ~ 16100 (~ 16000) in the most populated bin ($1 < p_T < 2$ GeV/ c) and less than ~ 900 (~ 300) in the highest p_T bin ($10 < p_T < 15$ GeV/ c).

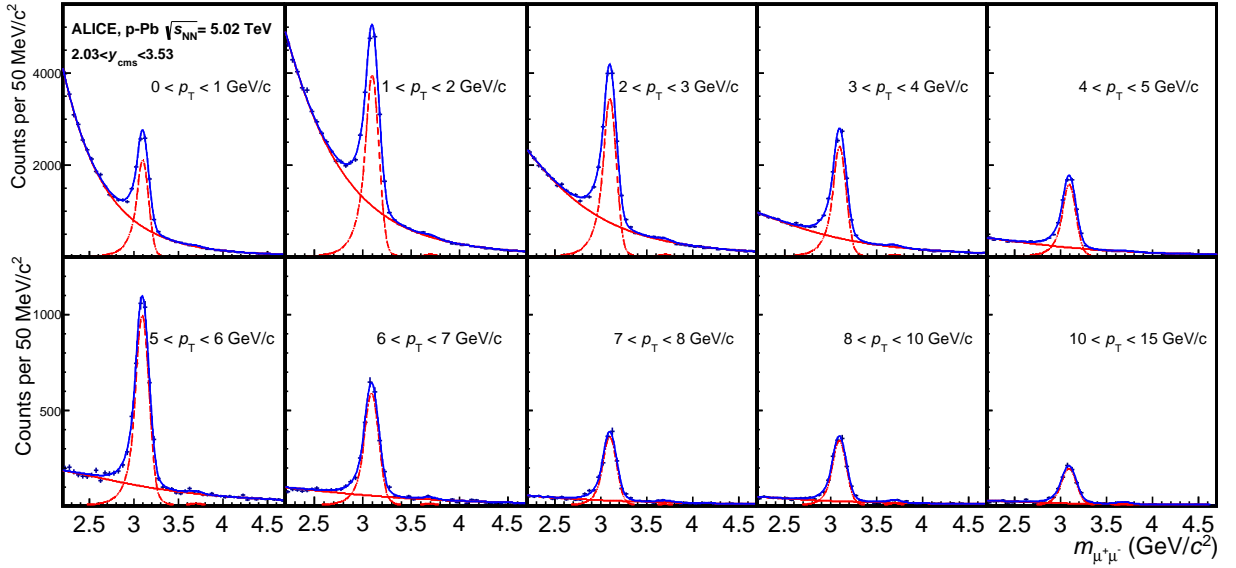


Fig. 3: The opposite-sign dimuon invariant mass spectra for the various p_T bins, relative to the p–Pb data sample (blue symbols). The fits shown in this Figure (blue curves) were performed by using the sum of extended Crystal Ball functions for the J/ψ and $\psi(2S)$ signals, and a variable width Gaussian for the background. The signal and background components are shown separately as red curves.

The J/ψ yields are then corrected for the product of acceptance times efficiency ($A \times \varepsilon$), evaluated by means of a MC simulation. J/ψ production is assumed to be unpolarized, as motivated by the small degree of polarization measured in pp collisions at $\sqrt{s} = 7$ TeV [47–49]. In the e^+e^- decay channel, $A \times \varepsilon$ is calculated using a MC simulation where J/ψ are injected into p–Pb collisions simulated with HIJING [50]. The decay products of the J/ψ are then propagated through a realistic description of the ALICE set-up, based on GEANT3.21 [51], taking into account the time evolution of the detector performance. Finally, J/ψ candidates are reconstructed with the same procedure applied to data. The p_T -integrated $A \times \varepsilon$ factor amounts to 8.9%. Its p_T -dependence exhibits a minimum ($\sim 7.5\%$) around $p_T = 2$ GeV/c, due to the kinematical acceptance, and it reaches $\sim 12\%$ at high p_T . The integrated value of $A \times \varepsilon$ is affected by a 3% systematic uncertainty related to the choice of the J/ψ p_T - and y -distributions used in the MC simulation. This value is obtained using as input several distributions, determined by varying within uncertainties the differential spectra extracted from the ALICE p–Pb data themselves. For p_T -differential studies, the values of $A \times \varepsilon$ are found to be sensitive only at a sub-percent level to the adopted input p_T - and y -distributions. A further small systematic uncertainty reaching 1.5% in the highest p_T interval and related to the statistical uncertainty of the MC sample is also introduced. The systematic uncertainty on the dielectron reconstruction efficiency is strongly dominated by the particle identification uncertainty and amounts to 4%. It was obtained by comparing the single track reconstruction efficiency for topologically identified positrons and electrons from photon conversions with the corresponding MC quantities. In the dimuon analysis, the J/ψ $A \times \varepsilon$ is obtained with a MC simulation, by generating signal-only samples, tracking them in the experimental set-up modeled with GEANT3.21 and using the same reconstruction procedure applied to data. The use of a pure signal MC is justified, since the tracking efficiency does not show a dependence on the hadronic multiplicity of the collision. A realistic description of the set-up is adopted, including the time evolution of the efficiencies of tracking and triggering detectors. As for the dielectron analysis, the differential distributions used as an input to the MC are tuned directly on the data. The J/ψ $A \times \varepsilon$ values, integrated over p_T , are 25.4% and 17.1% for p–Pb and Pb–p respectively [8], and exhibit a dependence on transverse momentum, being of the order of $\sim 24\%$ ($\sim 16\%$) for p–Pb (Pb–p) at low p_T and reaches $\sim 50\%$ ($\sim 35\%$) in the highest p_T bin ($10 < p_T < 15$ GeV/c). The systematically lower $A \times \varepsilon$ values in Pb–p reflect the smaller detector

Source	$\sigma_{pPb}^{J/\psi}, R_{pPb}$ $-1.37 < y_{\text{cms}} < 0.43$	$\sigma_{pPb}^{J/\psi}, R_{pPb}$ $2.03 < y_{\text{cms}} < 3.53$	$\sigma_{Pbp}^{J/\psi}, R_{Pbp}$ $-4.46 < y_{\text{cms}} < -2.96$
<i>Uncorrelated</i>			
Tracking efficiency ($\mu^+\mu^-$)	-	4	6
Trigger efficiency ($\mu^+\mu^-$)	-	2.7 – 4.1	2.7 – 4.1
Matching efficiency ($\mu^+\mu^-$)	-	1	1
Reconstruction efficiency (e^+e^-)	4	-	-
Signal extraction	5.5 – 12.6	2 – 2.5	2 – 3.6
MC input	0.3 – 1.5	0.1 – 0.4	0.1 – 1.4
$\sigma_{pp}^{J/\psi}$	4.8 – 15.7	5.2 – 9.2	5.2 – 9.2
<i>Partially correlated</i>			
$\sigma_{pp}^{J/\psi}$ (corr. vs y and p_T)	-	2.8 – 5.9	2 – 5.6
<i>Correlated</i>			
B.R. ($J/\psi \rightarrow l^+l^-$)	1	1	1
\mathcal{L}_{int} (corr. vs. p_T , uncorr. vs. y)	3.3	3.4	3.1
\mathcal{L}_{int} (corr. vs. y and p_T)	1.6	1.6	1.6
$\sigma_{pp}^{J/\psi}$	16.6	5.2	5.2

Table 1: Systematic uncertainties (in percent) on the measurement of inclusive J/ψ cross sections and nuclear modification factors. For p_T -dependent uncertainties, the minimum and maximum values are given. The degree of correlation (uncorrelated, partially correlated, correlated) refers to the p_T -dependence, unless specified otherwise. It cannot be excluded that a degree of correlation, difficult to quantify, is present also in uncertainties currently labelled as uncorrelated. Uncertainties on \mathcal{L}_{int} and branching ratios are relevant for cross sections, while those on $\sigma_{pp}^{J/\psi}$ contribute only to the uncertainty on the nuclear modification factors. \mathcal{L}_{int} uncertainties are split into two components, respectively uncorrelated and correlated between p–Pb and Pb–p, as detailed in [43].

efficiency in the corresponding data taking period. The systematic uncertainty on the integrated $A \times \varepsilon$ due to the input shapes is 1.5% for both p–Pb and Pb–p, and has been estimated using various distributions obtained from data and corresponding to smaller intervals in y , p_T and centrality (see [8] for details). For p_T -differential studies, the corresponding uncertainties are below 1.5%. The uncertainty on the dimuon tracking efficiency amounts to 4% (6%) for p–Pb (Pb–p) and is taken as constant for the full p_T range. It is evaluated by combining the uncertainties on single muon tracking efficiencies, considered as uncorrelated. The efficiency of each tracking plane is obtained using the redundancy of the tracking system (two independent planes per station) and then single muon efficiencies for the full tracking system are calculated according to the tracking algorithm [52]. Their uncertainty is determined by comparing the efficiency obtained with tracks from MC and real data. The systematic uncertainty on the dimuon trigger efficiency includes: (i) a contribution due to the uncertainty in the evaluation of the trigger detector efficiency ($\sim 2\%$, independent of p_T); (ii) a 0.5 – 3% p_T -dependent contribution (2% for the integrated efficiency), related to small differences in the trigger response function between data and MC in the region close to the trigger threshold; (iii) a 0.5 – 3.5% p_T -dependent contribution due to a small fraction of opposite-sign pairs which were misidentified as like-sign by the trigger system. Finally, a $\sim 1\%$ uncertainty, independent of p_T , is included, due to the choice of the value of the χ^2 cut applied to the matching of tracks reconstructed in the muon tracking and triggering systems.

The differential cross section for inclusive J/ψ production is defined as:

$$\frac{d^2\sigma_{pPb}^{J/\psi}}{dydp_T} = \frac{N_{J/\psi}(\Delta y, \Delta p_T)}{\mathcal{L}_{int}^{pPb} \cdot (A \times \varepsilon)_{(\Delta y, \Delta p_T)} \cdot \text{B.R.}(J/\psi \rightarrow l^+l^-) \cdot \Delta y \cdot \Delta p_T} \quad (1)$$

where $N_{J/\psi}(\Delta y, \Delta p_T)$ is the number of J/ψ for a given Δy and Δp_T interval. The branching ratio to dilep-

tons, $B.R.(J/\psi \rightarrow l^+l^-)$, is $5.94 \pm 0.06\%$ ($5.93 \pm 0.06\%$) for the dielectron (dimuon) decay [53]. The integrated luminosity, $\mathcal{L}_{\text{int}}^{\text{pPb}}$, is the ratio between N_{MB} , the number of MB collisions, and $\sigma_{\text{pPb}}^{\text{MB}}$, the corresponding cross section, measured in a van der Meer scan to be 2.09 ± 0.07 b for the p–Pb configuration and 2.12 ± 0.07 b for the Pb–p case [43]. The luminosity is also independently determined by means of a second signal based on a Čerenkov counter [39], as described in [43]. The two measurements differ by at most 1% throughout the whole data-taking period and such a value is quadratically added to the luminosity uncertainty. Finally, since the dimuon analysis is based on a sample of N_{DIMU} dimuon triggered events, the number of equivalent MB collisions is computed as $N_{\text{MB}} = F \cdot N_{\text{DIMU}}$, where F is a factor accounting for the probability of having a dimuon trigger when the MB condition is satisfied and for the small ($\sim 2\%$) pile-up probability in the corresponding data sample. The systematic uncertainty on this quantity, quadratically added to the other luminosity uncertainties, is 1% and originates from the comparison between the different approaches used for its evaluation [8]. A summary of the systematic uncertainties can be found in Table 1. The differential inclusive J/ψ cross sections are shown in Fig. 4, in the ranges $p_T < 10$ GeV/c for the dielectron analysis and $p_T < 15$ GeV/c for the dimuon analysis. The numerical values can be found in Table 2.

For the dielectron analysis, the p_T -integrated cross section was also determined, obtaining

$$d\sigma_{\text{pPb}}^{J/\psi}/dy(-1.37 < y_{\text{cms}} < 0.43) = 909 \pm 78(\text{stat.}) \pm 71(\text{syst.}) \mu\text{b}.$$

The corresponding p_T -integrated cross sections for the dimuon analysis were published in [8].

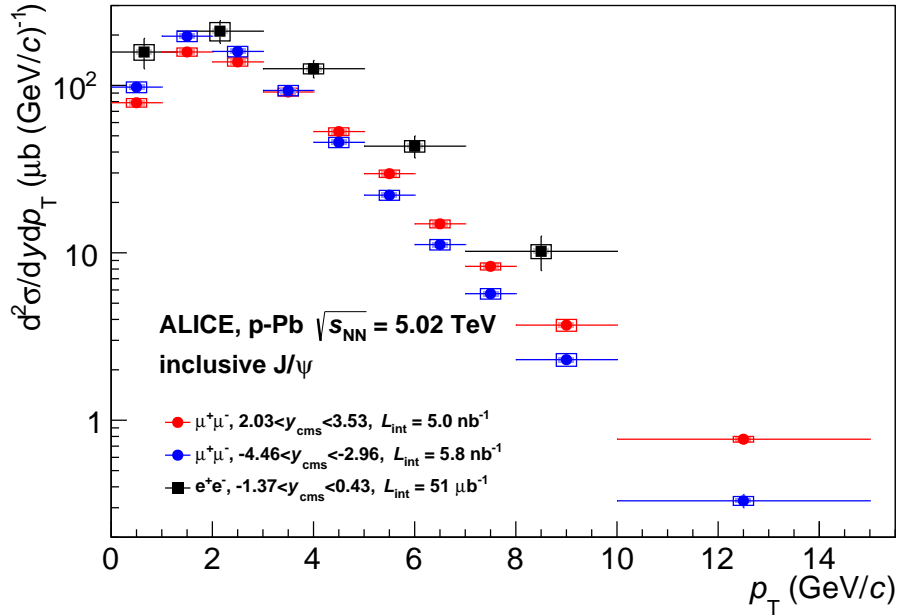


Fig. 4: p_T -differential inclusive J/ψ cross sections for the various rapidity regions under study. The vertical error bars correspond to the statistical uncertainties, while open boxes represent the uncorrelated systematic uncertainties and the shaded boxes the quadratic sum of the fully and partially correlated ones. The numerical values can be read in Table 2. The horizontal bars correspond to the widths of the p_T bins.

Starting from the p_T -differential J/ψ cross sections it is possible to evaluate, as additional information, the mean p_T ($\langle p_T \rangle$) for the various y -ranges, by means of fits based on the empirical function:

$$\frac{d^2\sigma_{\text{pPb}}^{J/\psi}}{dy dp_T} = C \times \frac{p_T}{\left[1 + \left(\frac{p_T}{p_0}\right)^2\right]^n} \quad (2)$$

p_T (GeV/c)	$d^2\sigma_{pPb}^{J/\psi}/dydp_T$ ($\mu\text{b}/(\text{GeV}/c)$)	p_T (GeV/c)	R_{pPb}	$d^2\sigma_{pp}^{J/\psi}/dydp_T$ (interpol.) ($\mu\text{b}/(\text{GeV}/c)$)
$-4.46 < y_{\text{cms}} < -2.96$ ($\mu^+\mu^-$)				
[0; 1]	$97.7 \pm 2.0 \pm 7.2 \pm 3.5$	[0; 1]	$0.96 \pm 0.02 \pm 0.09 \pm 0.03 \pm 0.06$	$0.490 \pm 0.029 \pm 0.017 \pm 0.026$
[1; 2]	$196.8 \pm 2.7 \pm 14.3 \pm 7.1$	[1; 2]	$1.06 \pm 0.01 \pm 0.10 \pm 0.04 \pm 0.07$	$0.892 \pm 0.048 \pm 0.030 \pm 0.046$
[2; 3]	$159.6 \pm 2.1 \pm 11.6 \pm 5.8$	[2; 3]	$1.11 \pm 0.01 \pm 0.10 \pm 0.04 \pm 0.07$	$0.693 \pm 0.036 \pm 0.025 \pm 0.036$
[3; 4]	$93.3 \pm 1.6 \pm 6.7 \pm 3.4$	[3; 4]	$1.16 \pm 0.02 \pm 0.10 \pm 0.04 \pm 0.07$	$0.388 \pm 0.021 \pm 0.012 \pm 0.020$
[4; 5]	$45.7 \pm 1.0 \pm 3.2 \pm 1.7$	[4; 5]	$1.17 \pm 0.02 \pm 0.11 \pm 0.03 \pm 0.07$	$0.187 \pm 0.011 \pm 0.004 \pm 0.010$
[5; 6]	$22.1 \pm 0.5 \pm 1.6 \pm 0.8$	[5; 6]	$1.13 \pm 0.03 \pm 0.12 \pm 0.02 \pm 0.07$	$0.094 \pm 0.007 \pm 0.002 \pm 0.005$
[6; 7]	$11.2 \pm 0.4 \pm 0.8 \pm 0.4$	[6; 8]	$1.27 \pm 0.03 \pm 0.14 \pm 0.08 \pm 0.08$	$0.032 \pm 0.003 \pm 0.002 \pm 0.002$
[7; 8]	$5.7 \pm 0.3 \pm 0.4 \pm 0.2$			
[8; 10]	$2.3 \pm 0.1 \pm 0.2 \pm 0.1$			
[10; 15]	$0.33 \pm 0.03 \pm 0.03 \pm 0.01$			
$-1.37 < y_{\text{cms}} < 0.43$ (e^+e^-)				
[0; 1.3]	$158 \pm 33 \pm 17 \pm 6$	[0; 1.3]	$0.81 \pm 0.17 \pm 0.10 \pm 0.14$	$0.94 \pm 0.07 \pm 0.16$
[1.3; 3]	$211 \pm 33 \pm 26 \pm 8$	[1.3; 3]	$0.64 \pm 0.10 \pm 0.09 \pm 0.11$	$1.60 \pm 0.08 \pm 0.26$
[3; 5]	$126 \pm 15 \pm 9 \pm 5$	[3; 5]	$0.77 \pm 0.09 \pm 0.07 \pm 0.13$	$0.79 \pm 0.05 \pm 0.13$
[5; 7]	$43.4 \pm 6.5 \pm 3.4 \pm 1.7$	[5; 7]	$0.89 \pm 0.13 \pm 0.13 \pm 0.15$	$0.23 \pm 0.03 \pm 0.04$
[7; 10]	$10.2 \pm 2.4 \pm 1.0 \pm 0.4$	[7; 10]	$0.89 \pm 0.21 \pm 0.16 \pm 0.15$	$0.06 \pm 0.01 \pm 0.01$
$2.03 < y_{\text{cms}} < 3.53$ ($\mu^+\mu^-$)				
[0; 1]	$78.8 \pm 1.5 \pm 4.6 \pm 3.1$	[0; 1]	$0.61 \pm 0.01 \pm 0.05 \pm 0.02 \pm 0.04$	$0.624 \pm 0.036 \pm 0.025 \pm 0.032$
[1; 2]	$158.4 \pm 2.2 \pm 9.0 \pm 6.2$	[1; 2]	$0.64 \pm 0.01 \pm 0.05 \pm 0.02 \pm 0.04$	$1.197 \pm 0.064 \pm 0.046 \pm 0.062$
[2; 3]	$138.2 \pm 1.9 \pm 7.9 \pm 5.4$	[2; 3]	$0.68 \pm 0.01 \pm 0.05 \pm 0.03 \pm 0.04$	$0.980 \pm 0.051 \pm 0.039 \pm 0.051$
[3; 4]	$91.3 \pm 1.4 \pm 5.0 \pm 3.6$	[3; 4]	$0.76 \pm 0.01 \pm 0.06 \pm 0.03 \pm 0.05$	$0.579 \pm 0.032 \pm 0.022 \pm 0.030$
[4; 5]	$53.0 \pm 0.9 \pm 2.8 \pm 2.1$	[4; 5]	$0.87 \pm 0.02 \pm 0.07 \pm 0.02 \pm 0.06$	$0.294 \pm 0.017 \pm 0.008 \pm 0.015$
[5; 6]	$29.7 \pm 0.6 \pm 1.6 \pm 1.1$	[5; 6]	$0.91 \pm 0.02 \pm 0.08 \pm 0.03 \pm 0.06$	$0.156 \pm 0.011 \pm 0.005 \pm 0.008$
[6; 7]	$14.9 \pm 0.4 \pm 0.8 \pm 0.6$	[6; 8]	$0.98 \pm 0.02 \pm 0.09 \pm 0.05 \pm 0.06$	$0.057 \pm 0.005 \pm 0.003 \pm 0.003$
[7; 8]	$8.3 \pm 0.3 \pm 0.5 \pm 0.3$			
[8; 10]	$3.7 \pm 0.1 \pm 0.2 \pm 0.1$			
[10; 15]	$0.77 \pm 0.03 \pm 0.05 \pm 0.03$			

Table 2: Summary of the results on the inclusive J/ψ differential cross sections and nuclear modification factors for p–Pb collisions. The results of the cross section interpolation for pp collisions are also shown. For p–Pb cross section results, the first quoted uncertainty is statistical. The following uncertainties are systematic, the second one being p_T -uncorrelated and the third one p_T -correlated. For R_{pPb} the first quoted uncertainty is statistical. The following uncertainties are systematic, the second one being p_T -uncorrelated. For dielectron results the third uncertainty is p_T -correlated, while for dimuon results the third uncertainty is partially p_T -correlated and the fourth is p_T -correlated. For the results on the interpolated pp cross section, the first quoted uncertainty combines statistical and p_T -uncorrelated systematic uncertainties. For dielectron results the second uncertainty is p_T -correlated systematic, while for dimuon results the second uncertainty is partially p_T -correlated, and the third is p_T -correlated.

where C , p_0 and n are free parameters. The quality of the fits is satisfactory ($\chi^2/\text{ndf} \sim 1$) and the resulting $\langle p_T \rangle$ values, computed for the measured p_T ranges, are

$$\begin{aligned}\langle p_T \rangle(-4.46 < y_{\text{cms}} < -2.96) &= 2.47 \pm 0.01(\text{stat.}) \pm 0.03(\text{syst.}) \text{ GeV}/c \\ \langle p_T \rangle(-1.37 < y_{\text{cms}} < 0.43) &= 2.86 \pm 0.15(\text{stat.}) \pm 0.10(\text{syst.}) \text{ GeV}/c \\ \langle p_T \rangle(2.03 < y_{\text{cms}} < 3.53) &= 2.77 \pm 0.01(\text{stat.}) \pm 0.03(\text{syst.}) \text{ GeV}/c\end{aligned}$$

The quoted uncertainties were obtained by performing fits including only statistical (or uncorrelated systematic) uncertainties on differential cross sections.

In order to perform a meaningful comparison of $\langle p_T \rangle$ results in the dielectron and dimuon analysis, the values from the dimuon analysis have also been extracted, with the same procedure detailed above, in the range $p_T < 10 \text{ GeV}/c$, obtaining results which are smaller by less than 2% with respect to the full p_T range. It is found that $\langle p_T \rangle$ is larger at central rapidity. Furthermore, the $\langle p_T \rangle$ measured at forward y_{cms} is significantly larger than at backward y_{cms} . This difference, which could be partly due to the slightly different $|y|$ -coverage, persists when $\langle p_T \rangle$ is calculated in the $|y_{\text{cms}}|$ region common to p-Pb and Pb-p ($2.96 < |y_{\text{cms}}| < 3.53$). The values obtained in this case are $2.58 \pm 0.02(\text{stat.}) \pm 0.04(\text{syst.}) \text{ GeV}/c$ and $2.69 \pm 0.02(\text{stat.}) \pm 0.03(\text{syst.}) \text{ GeV}/c$, respectively at backward and forward y_{cms} , and differ by $\sim 2\sigma$.

The J/ψ nuclear modification factor R_{pPb} is obtained as the ratio of the differential cross sections between proton-nucleus and proton-proton collisions, normalized to A_{Pb} :

$$R_{pPb}(y, p_T) = \frac{d^2\sigma_{pPb}^{J/\psi}/dydp_T}{A_{Pb} \cdot d^2\sigma_{pp}^{J/\psi}/dydp_T} \quad (3)$$

Since no pp data are available at $\sqrt{s} = 5.02 \text{ TeV}$, the $d^2\sigma_{pp}^{J/\psi}/dydp_T$ reference cross sections were obtained by means of an interpolation/extrapolation procedure. For the dielectron analysis, the starting point of the interpolation procedure is the determination of $d\sigma/dy$ for inclusive J/ψ in pp collisions at $y_{\text{cms}} \sim 0$ and $\sqrt{s} = 5.02 \text{ TeV}$, carried out as for the analysis described in [30]. Available mid-rapidity data at $\sqrt{s} = 0.2$ [54], 1.96 [55], 2.76 [56] and 7 TeV [44] are interpolated using several empirical functions (exponential, logarithmic and power-law, covering in this way the various possibilities for the curvature of the \sqrt{s} -dependence) obtaining $d\sigma/dy = 6.19 \pm 1.03 \mu\text{b}$. Even if the y_{cms} range covered in this analysis is shifted by 0.465 units with respect to mid-rapidity, the rapidity-dependence of the cross section is negligible compared to the uncertainty on the interpolation procedure. Then, a method similar to the one in [57] is applied to derive the p_T -differential cross section. It is based on the empirical observation that pp and $p\bar{p}$ results on differential spectra obtained at various collision energies and in different rapidity ranges [44, 48, 54, 55, 58] exhibit scaling properties when plotted as a function of $p_T/\langle p_T \rangle$. The normalized spectra, with the statistical and the bin-by-bin uncorrelated systematic uncertainties added in quadrature, can be fitted with a one-parameter function described in [57]. The p_T -differential cross sections at mid-rapidity and $\sqrt{s} = 5.02 \text{ TeV}$ can then be obtained by rescaling the fitted universal distribution using the previously estimated $d\sigma/dy$ and its corresponding $\langle p_T \rangle$. The latter value is obtained by an interpolation of the energy-dependence of $\langle p_T \rangle$ values evaluated fitting the available experimental mid-rapidity results [44, 54, 55] with exponential, logarithmic and power-law functions. One obtains in this way, in the range $p_T < 10 \text{ GeV}/c$, $\langle p_T \rangle = 2.81 \pm 0.10 \text{ GeV}/c$ as an average of the results calculated with the various empirical functions. As outlined above for $d\sigma/dy$, the 0.465 y -unit shift of the data with respect to mid-rapidity has a negligible effect also on $\langle p_T \rangle$.

For the dimuon analysis, thanks to the smaller uncertainties with respect to mid-rapidity results, an approach equivalent to that described in [59], exclusively based on the ALICE data collected at $\sqrt{s} = 2.76 \text{ TeV}$ [56] and 7 TeV [60] in $2.5 < y_{\text{cms}} < 4$, $p_T < 8 \text{ GeV}/c$ has been used. The reference cross

sections are obtained with a two-step procedure, corresponding to an energy interpolation followed by a rapidity extrapolation. In the first step, for each p_T bin, the $d^2\sigma_{pp}^{J/\psi}/dydp_T$ values at $\sqrt{s} = 2.76$ and 7 TeV are interpolated, using three different empirical functions (linear, power-law and exponential) to estimate the cross section values at $\sqrt{s} = 5.02$ TeV. The central values are calculated as the average of the results obtained with the three functions, while the associated uncertainties come from the experimental uncertainties on the points used for the interpolation, added in quadrature to a contribution chosen as the maximum spread of the results from the different interpolating functions. In the second step, this result is extrapolated from $2.5 < y_{cms} < 4$ to the p–Pb and Pb–p y_{cms} ranges, using the scaling factors for the p_T -integrated cross sections computed in [59]. Finally, since the LHCb Collaboration has shown that the J/ψ p_T distributions slightly depend on y_{cms} [48] in the rapidity range covered in the dimuon analysis, a p_T -dependent correction tuned on these data (10% maximum at large p_T) is applied.

The inclusive J/ψ nuclear modification factor is shown in Fig. 5 for the three rapidity regions under study. The numerical values of R_{pPb} , as well as the results of the interpolation procedure for the estimate of the pp cross sections, can be found in Table 2. For the dimuon analysis, the evaluation of R_{pPb} is restricted to $p_T < 8$ GeV/c, the region covered by the pp measurements used in the evaluation of the reference cross sections. The sources of systematic uncertainties on R_{pPb} and their values are summarized in Table 1. The terms related to the pp reference cross sections contribute to uncorrelated, partially or fully correlated uncertainties on R_{pPb} , depending on their origin. In particular, for the dimuon analysis: (i) the statistical and p_T -uncorrelated systematic uncertainties on the $\sqrt{s} = 2.76$ and 7 TeV pp data contribute to the uncorrelated uncertainty; (ii) the spread of the results obtained with various interpolating/extrapolating functions in \sqrt{s} and y_{cms} contribute to the partially correlated uncertainty; (iii) the \sqrt{s} -correlated uncertainties between the $\sqrt{s} = 2.76$ and 7 TeV pp data contribute to the correlated uncertainty. At forward and mid-rapidity the J/ψ R_{pPb} shows a clear suppression at low p_T , vanishing at high p_T . At backward rapidity no suppression is present, within uncertainties.

For the dielectron analysis, the p_T -integrated nuclear modification factor was also calculated, carrying out the signal extraction procedure on the p_T -integrated invariant mass spectrum. The obtained value

$$R_{pPb} = 0.71 \pm 0.06(\text{stat.}) \pm 0.13(\text{syst.})$$

is consistent with the forward rapidity ($2.03 < y_{cms} < 3.53$) dimuon result, and smaller than the backward one ($-4.46 < y_{cms} < -2.96$) by $\sim 2\sigma$ [8].

In Fig. 5 predictions from various models are compared to the data. A calculation based on the next-to-leading order (NLO) Color Evaporation Model (CEM) for the prompt J/ψ production and the EPS09 shadowing parametrization [33] reproduces within uncertainties the p_T -dependence and the amplitude of the suppression for $p_T > 1.5$ GeV/c in the three rapidity regions under study. The theoretical uncertainties arise from the uncertainties on EPS09 as well as on the values of charm quark mass and of the renormalization and factorization scales used for the cross section calculation. Data are also compared to two calculations based on a parametrization of experimental results on prompt J/ψ production in pp collisions and including the effects of coherent energy loss [35] in the cold nuclear medium. One of the calculations includes only coherent energy loss, while the other combines coherent energy loss with EPS09 shadowing. The uncertainty bands include, for the coherent energy loss mechanism, a variation of both the q_0 parameter (gluon transport coefficient evaluated at $x = 0.01$) and the parametrization of the production cross section. At forward rapidity the pure energy loss scenario predicts a much steeper p_T -dependence, while better agreement is found when the EPS09 contribution is included. However, at low p_T , a discrepancy between data and both calculations is observed. Also at mid-rapidity the coherent energy loss model including the EPS09 contribution better describes the data, although the larger uncertainties prevent a firm conclusion. The same features can be observed at backward rapidity, where the calculation including coherent energy loss and shadowing agrees with the data in showing weak nuclear effects on J/ψ production. Finally, the results at central and forward rapidities are compared with

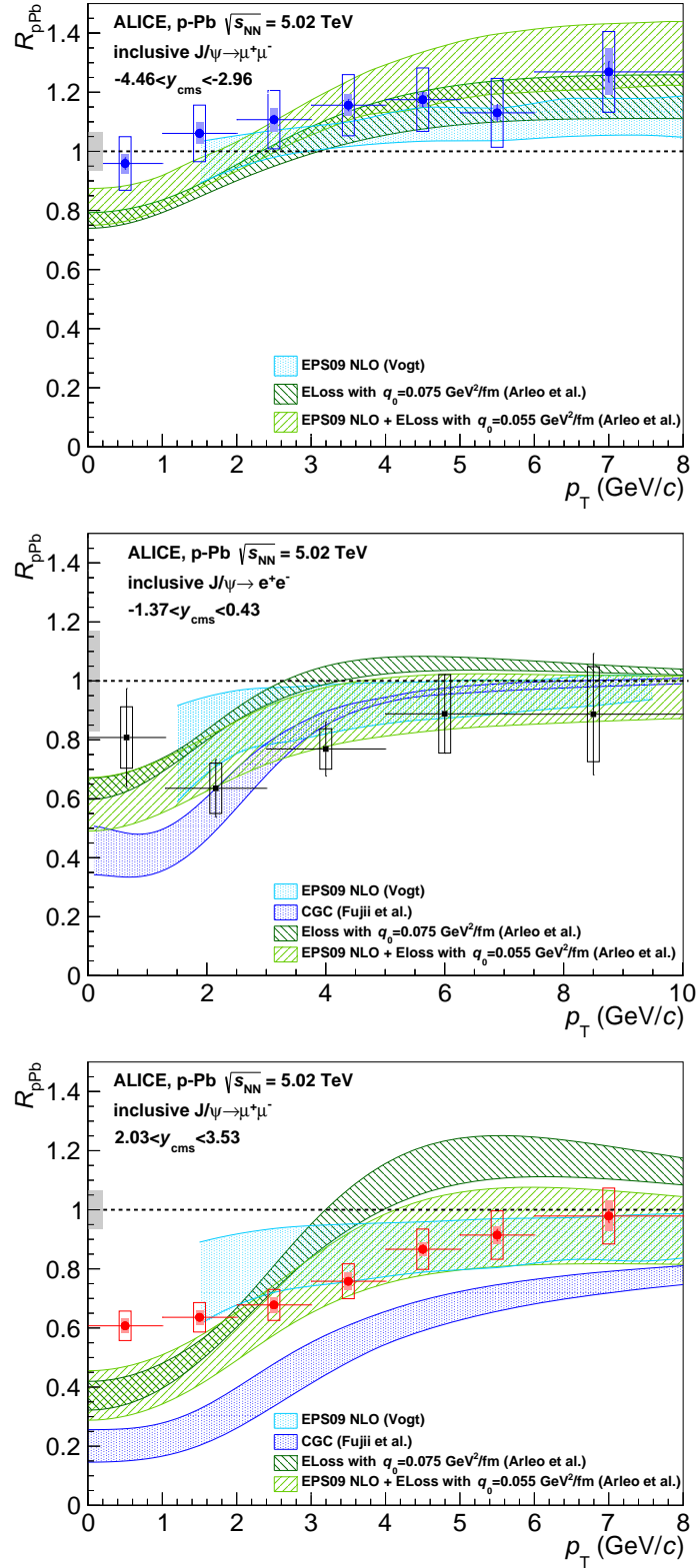


Fig. 5: The J/ψ nuclear modification factor as a function of p_T at backward (top), mid (center) and forward (bottom) rapidities. Statistical uncertainties are represented by vertical error bars, while open boxes correspond to uncorrelated uncertainties and the shaded areas to uncertainties partially correlated in p_T . The boxes around $R_{pPb} = 1$ show the size of the correlated uncertainties. The horizontal bars correspond to the widths of the p_T bins. Results from various models are also shown, including a pure shadowing calculation [33] based on the EPS09 parameterization, a CGC-inspired model [36], and the results of the coherent energy loss calculation [35], with or without the inclusion of an EPS09 shadowing contribution.

a prediction based on the CGC framework and using CEM for the prompt J/ψ production [36]. In the backward rapidity region, higher gluon x in the nucleus are probed and the CGC model is out of its range of applicability. The quoted uncertainties are related to the choices of Q_s^2 and of the charm quark mass. While the model is in fair agreement with mid-rapidity data, it clearly underpredicts the J/ψ R_{pPb} in the full p_T range at forward rapidity.

The theoretical calculations discussed above are carried out for prompt J/ψ (i.e., direct J/ψ and the contribution from χ_c and $\psi(2S)$ decays), while the measurements are for inclusive J/ψ which include a non-prompt contribution from B-hadron decays. The contribution of the latter source to R_{pPb}^{incl} can be evaluated from the measured fraction f_B of non-prompt to prompt J/ψ production in pp collisions and on the suppression $R_{pPb}^{\text{non-prompt}}$ of non-prompt J/ψ in p–Pb collisions. More in detail, in the range $2 < y_{\text{cms}} < 4.5$, the fraction f_B measured by LHCb in pp collisions at $\sqrt{s} = 7$ TeV, increases from 0.08 to 0.22 from $p_T = 0$ to 8 GeV/c [48]. This quantity has a small variation within the y_{cms} range covered and is also not strongly \sqrt{s} -dependent (similar values are obtained for $\sqrt{s} = 8$ TeV [58]). At mid-rapidity, f_B was measured by ALICE in pp collisions at $\sqrt{s} = 7$ TeV and ranges from 0.10 to 0.44 for p_T increasing from 1.3 to 10 GeV/c [61]. $R_{pPb}^{\text{non-prompt}}$ was measured at $\sqrt{s_{\text{NN}}} = 5.02$ TeV by LHCb, integrated over p_T , obtaining $0.83 \pm 0.02 \pm 0.08$ for $2.5 < y_{\text{cms}} < 4$ and $0.98 \pm 0.06 \pm 0.10$ for $-4 < y_{\text{cms}} < -2.5$ [9]. Assuming for each p_T -bin a variation of $R_{pPb}^{\text{non-prompt}}$ between 0.6 and 1.3, a conservative choice due to the unavailability of a p_T -differential result, and considering the p_T -dependence of f_B at $\sqrt{s} = 7$ TeV, one can extract R_{pPb}^{prompt} as $R_{pPb}^{\text{prompt}} = R_{pPb}^{\text{incl}} + f_B \cdot (R_{pPb}^{\text{incl}} - R_{pPb}^{\text{non-prompt}})$. The maximum differences between the inclusive and prompt R_{pPb} obtained in this way are, for low and high p_T : (i) 3 and 10% at backward rapidity; (ii) 11 and 16% at central rapidity; (iii) 10 and 8% at forward rapidity. These variations are, at most, of the same order of magnitude as the quoted uncertainties on inclusive R_{pPb} .

The R_{pPb} results shown in this paper can be considered as a valuable tool to improve our understanding of the contribution of CNM to the suppression of the J/ψ yields observed in Pb–Pb [30, 31]. Indeed, as verified in [8] for the dimuon analysis, in Pb–Pb collisions the Bjorken- x ranges probed by the J/ψ production process in the two colliding nuclei, assuming a $gg \rightarrow J/\psi$ ($2 \rightarrow 1$) [62] mechanism, are shifted by only $\sim 10\%$ with respect to the corresponding intervals for p–Pb and Pb–p, despite the different energy ($\sqrt{s_{\text{NN}}} = 2.76$ TeV) and the slightly different y_{cms} range ($2.5 < y < 4$) for Pb–Pb. A similar conclusion holds at mid-rapidity, where the covered x -intervals, calculated for $p_T = \langle p_T \rangle$, are $6.1 \times 10^{-4} < x < 3.0 \times 10^{-3}$ and $7.0 \times 10^{-4} < x < 3.5 \times 10^{-3}$ for p–Pb and Pb–Pb collisions, respectively. Under the assumption that shadowing is the main CNM-related mechanism that plays a role in the J/ψ production and that its effect on the two colliding nuclei in Pb–Pb collisions can be factorized, the product $R_{pPb} \times R_{PbP}$ (R_{pPb}^2) can be considered as an estimate of CNM effects in Pb–Pb collisions at forward (central) rapidity [63, 64]. This conclusion holds not only for the $2 \rightarrow 1$ production process but also when the more general $2 \rightarrow 2$ mechanism ($gg \rightarrow J/\psi g$) is considered.

In Fig. 6 the comparison of the measured R_{pPb} with the quantities defined above is carried out. Such a comparison should be considered as qualitative, in view of the slight x -mismatch detailed above and of the fact that, at mid-rapidity, the centrality ranges probed in p–Pb and Pb–Pb are not the same (0–100% and 0–50%, respectively). In both rapidity regions, the extrapolation of CNM effects shows a clear p_T -dependence, corresponding to a strong suppression at low p_T , which vanishes for large transverse momenta. At low p_T and central rapidity, there might be an indication for a Pb–Pb suppression smaller than the CNM extrapolation, consistent with the presence of a contribution related to the (re)combination of $c\bar{c}$ pairs [30], taking place in the hot medium. A similar effect can be seen at forward rapidity. At large p_T and forward rapidity, the observed suppression in Pb–Pb collisions is much larger than CNM extrapolations, showing that, in this transverse-momentum region, suppression effects in hot matter, possibly related to color screening, become dominant.

Finally, a more direct comparison of Pb–Pb results with the CNM extrapolation can be obtained by defining the ratio $S_{J/\psi} = R_{pPb}/(R_{pPb} \times R_{PbP})$. Such a quantity, for forward rapidity results, is shown in

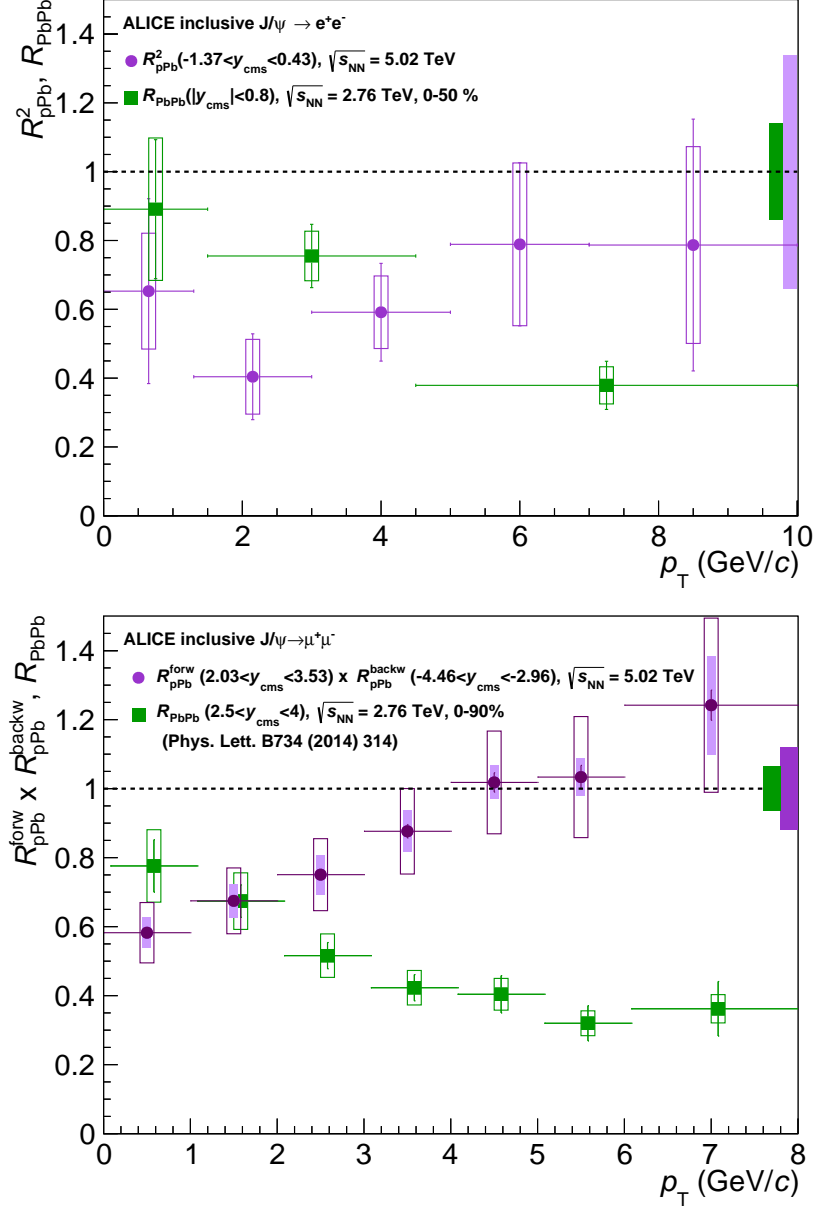


Fig. 6: The estimate of the p_T -dependence of CNM effects in Pb-Pb, calculated as R_{pPb}^2 for mid-rapidity data (top) and as $R_{pPb}^{forw} \times R_{pPb}^{backw}$ (bottom) at forward rapidity. The quantities are compared to R_{PbPb} measured in Pb-Pb collisions in the (approximately) corresponding y -ranges [30, 31]. The vertical error bars correspond to the statistical uncertainties, the open boxes (shaded areas) represent p_T -uncorrelated (partially correlated) systematic uncertainties, while the boxes around $R_{pPb} = 1$ show the size of the correlated uncertainties. The horizontal bars correspond to the widths of the p_T bins. The Pb-Pb points in the bottom panel were slightly displaced in p_T , to improve visibility.

Fig. 7 and confirms the main features detailed above, i.e., a strong suppression of J/ψ at large p_T , and a hint for an enhancement at low p_T . At central rapidity, due to the sizeable uncertainties on both p–Pb and Pb–Pb results, only the p_T -integrated ratio can be obtained. Using the R_{PbPb} in the 0-90% centrality range [30], and the integrated R_{pPb} given above, one gets $1.43 \pm 0.26(\text{stat}) \pm 0.56(\text{syst})$. More precise measurements are needed to draw a firm conclusion in this rapidity range.

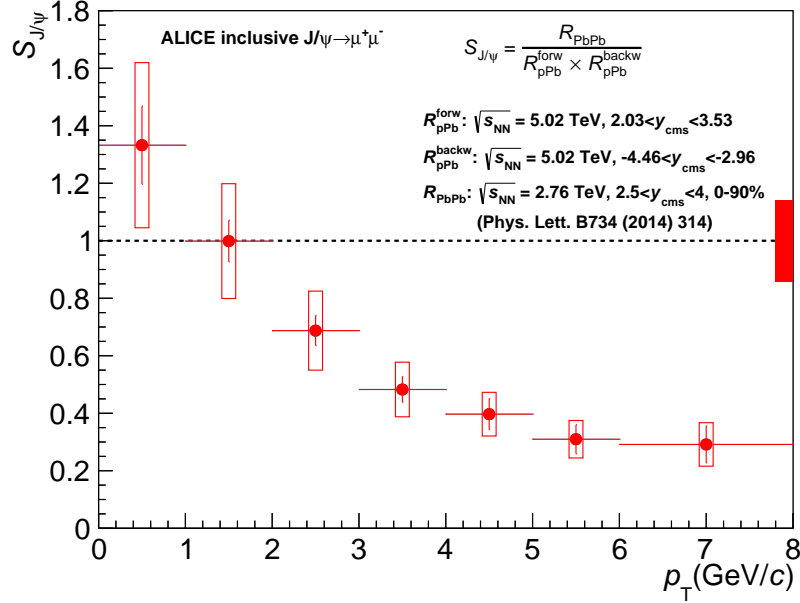


Fig. 7: The ratio between R_{PbPb} for inclusive J/ψ at forward rapidity and the product $R_{pPb} \times R_{pPb}$ of the nuclear modification factors at forward and backward rapidity. None of the uncertainties cancels out in the ratio. Statistical uncertainties are shown as vertical error bars, while the boxes around the points represent a quadratic combination of uncorrelated and partially correlated systematic uncertainties. The box around $S_{J/\psi} = 1$ corresponds to correlated uncertainties. The horizontal bars coincide with the widths of the p_T bins.

In summary, we have presented results on the inclusive J/ψ production in p–Pb collisions at $\sqrt{s_{NN}} = 5.02$ TeV. The p_T -differential cross sections, the $\langle p_T \rangle$ and the nuclear modification factors have been evaluated in three rapidity regions: $-4.46 < y_{cms} < -2.96$, $-1.37 < y_{cms} < 0.43$ and $2.03 < y_{cms} < 3.53$. At forward and mid-rapidity a significant suppression is observed at low p_T , with a vanishing trend at high p_T . At backward rapidity no significant suppression or enhancement is visible. Comparisons with theoretical models based on a combination of nuclear shadowing and coherent energy loss effects provide a fair description of the observed patterns, except at forward rapidity and low transverse momentum. These results can be used to provide a qualitative estimate of the influence of cold nuclear matter effects on the J/ψ suppression observed in Pb–Pb collisions. Under the assumption that shadowing represents the main CNM contribution, we find that it cannot account for the observed suppression in Pb–Pb at high p_T . At low p_T , the observed CNM effects alone may suggest a suppression larger than that observed in Pb–Pb, which is consistent with the presence of a charm quark (re)combination component to the J/ψ production in nucleus-nucleus collisions.

Acknowledgements

The ALICE Collaboration would like to thank all its engineers and technicians for their invaluable contributions to the construction of the experiment and the CERN accelerator teams for the outstanding performance of the LHC complex. The ALICE Collaboration gratefully acknowledges the resources and support provided by all Grid centres and the Worldwide LHC Computing Grid (WLCG) collaboration. The ALICE Collaboration acknowledges the following funding agencies for their support

in building and running the ALICE detector: State Committee of Science, World Federation of Scientists (WFS) and Swiss Fonds Kidagan, Armenia, Conselho Nacional de Desenvolvimento Científico e Tecnológico (CNPq), Financiadora de Estudos e Projetos (FINEP), Fundação de Amparo à Pesquisa do Estado de São Paulo (FAPESP); National Natural Science Foundation of China (NSFC), the Chinese Ministry of Education (CMOE) and the Ministry of Science and Technology of China (MSTC); Ministry of Education and Youth of the Czech Republic; Danish Natural Science Research Council, the Carlsberg Foundation and the Danish National Research Foundation; The European Research Council under the European Community's Seventh Framework Programme; Helsinki Institute of Physics and the Academy of Finland; French CNRS-IN2P3, the 'Region Pays de Loire', 'Region Alsace', 'Region Auvergne' and CEA, France; German Bundesministerium für Bildung, Wissenschaft, Forschung und Technologie (BMBF) and the Helmholtz Association; General Secretariat for Research and Technology, Ministry of Development, Greece; Hungarian Országos Tudományos Kutatási Alapprogramok (OTKA) and National Office for Research and Technology (NKTH); Department of Atomic Energy and Department of Science and Technology of the Government of India; Istituto Nazionale di Fisica Nucleare (INFN) and Centro Fermi - Museo Storico della Fisica e Centro Studi e Ricerche "Enrico Fermi", Italy; MEXT Grant-in-Aid for Specially Promoted Research, Japan; Joint Institute for Nuclear Research, Dubna; National Research Foundation of Korea (NRF); Consejo Nacional de Ciencia y Tecnología (CONACYT), Dirección General de Asuntos del Personal Académico (DGAPA), México; Amérique Latine Formation académique European Commission (ALFA-EC) and the EPLANET Program (European Particle Physics Latin American Network) Stichting voor Fundamenteel Onderzoek der Materie (FOM) and the Nederlandse Organisatie voor Wetenschappelijk Onderzoek (NWO), Netherlands; Research Council of Norway (NFR); National Science Centre, Poland; Ministry of National Education/Institute for Atomic Physics and Consiliul Național al Cercetării Științifice - Executive Agency for Higher Education Research Development and Innovation Funding (CNCS-UEFISCDI) - Romania; Ministry of Education and Science of Russian Federation, Russian Academy of Sciences, Russian Federal Agency of Atomic Energy, Russian Federal Agency for Science and Innovations and The Russian Foundation for Basic Research; Ministry of Education of Slovakia; Department of Science and Technology, South Africa; Centro de Investigaciones Energéticas, Medioambientales y Tecnológicas (CIEMAT), E-Infrastructure shared between Europe and Latin America (EELA), Ministerio de Economía y Competitividad (MINECO) of Spain, Xunta de Galicia (Consellería de Educación), Centro de Aplicaciones Tecnológicas y Desarrollo Nuclear (CEADEN), Cubaenergía, Cuba, and IAEA (International Atomic Energy Agency); Swedish Research Council (VR) and Knut & Alice Wallenberg Foundation (KAW); Ukraine Ministry of Education and Science; United Kingdom Science and Technology Facilities Council (STFC); The United States Department of Energy, the United States National Science Foundation, the State of Texas, and the State of Ohio; Ministry of Science, Education and Sports of Croatia and Unity through Knowledge Fund, Croatia. Council of Scientific and Industrial Research (CSIR), New Delhi, India

References

- [1] T. Matsui and H. Satz, " J/ψ Suppression by Quark-Gluon Plasma Formation," *Phys.Lett.* **B178** (1986) 416.
- [2] C. Gerschel and J. Hüfner, "A Contribution to the Suppression of the J/ψ Meson Produced in High-Energy Nucleus Nucleus Collisions," *Phys.Lett.* **B207** (1988) 253–256.
- [3] NA50 Collaboration, B. Alessandro *et al.*, " J/ψ and ψ' production and their normal nuclear absorption in proton-nucleus collisions at 400-GeV," *Eur.Phys.J.* **C48** (2006) 329, arXiv:nucl-ex/0612012 [nucl-ex].
- [4] NA60 Collaboration, R. Arnaldi *et al.*, " J/ψ production in proton-nucleus collisions at 158 and 400 GeV," *Phys.Lett.* **B706** (2012) 263–267, arXiv:1004.5523 [nucl-ex].

- [5] **HERA-B** Collaboration, I. Abt *et al.*, “Kinematic distributions and nuclear effects of J/ψ production in 920-GeV fixed-target proton-nucleus collisions,” *Eur.Phys.J.* **C60** (2009) 525–542, arXiv:0812.0734 [hep-ex].
- [6] **E866** Collaboration, M. Leitch *et al.*, “Measurement of J/ψ and ψ' suppression in p-A collisions at 800-GeV/c,” *Phys.Rev.Lett.* **84** (2000) 3256–3260, arXiv:nucl-ex/9909007 [nucl-ex].
- [7] **PHENIX** Collaboration, A. Adare *et al.*, “Transverse-Momentum Dependence of the J/ψ Nuclear Modification in $d+Au$ Collisions at $\sqrt{s_{NN}} = 200$ GeV,” *Phys.Rev.* **C87** no. 3, (2013) 034904, arXiv:1204.0777 [nucl-ex].
- [8] **ALICE** Collaboration, B. B. Abelev *et al.*, “ J/ψ production and nuclear effects in p-Pb collisions at $\sqrt{s_{NN}} = 5.02$ TeV,” *JHEP* **1402** (2014) 073, arXiv:1308.6726 [nucl-ex].
- [9] **LHCb** Collaboration, R. Aaij *et al.*, “Study of J/ψ production and cold nuclear matter effects in pPb collisions at $\sqrt{s_{NN}} = 5$ TeV,” *JHEP* **1402** (2014) 072, arXiv:1308.6729 [nucl-ex].
- [10] G. T. Bodwin, E. Braaten, and G. P. Lepage, “Rigorous QCD analysis of inclusive annihilation and production of heavy quarkonium,” *Phys.Rev.* **D51** (1995) 1125–1171, arXiv:hep-ph/9407339 [hep-ph].
- [11] J. Amundson, O. J. Eboli, E. Gregores, and F. Halzen, “Quantitative tests of color evaporation: Charmonium production,” *Phys.Lett.* **B390** (1997) 323–328, arXiv:hep-ph/9605295 [hep-ph].
- [12] R. Baier and R. Ruckl, “Hadronic Production of J/ψ and Upsilon: Transverse Momentum Distributions,” *Phys.Lett.* **B102** (1981) 364.
- [13] K. Eskola, H. Paukkunen, and C. Salgado, “EPS09: A New Generation of NLO and LO Nuclear Parton Distribution Functions,” *JHEP* **0904** (2009) 065, arXiv:0902.4154 [hep-ph].
- [14] D. de Florian, R. Sassot, P. Zurita, and M. Stratmann, “Global Analysis of Nuclear Parton Distributions,” *Phys.Rev.* **D85** (2012) 074028, arXiv:1112.6324 [hep-ph].
- [15] M. Hirai, S. Kumano, and T.-H. Nagai, “Determination of nuclear parton distribution functions and their uncertainties in next-to-leading order,” *Phys.Rev.* **C76** (2007) 065207, arXiv:0709.3038 [hep-ph].
- [16] D. Kharzeev and K. Tuchin, “Signatures of the color glass condensate in J/ψ production off nuclear targets,” *Nucl.Phys.* **A770** (2006) 40–56, arXiv:hep-ph/0510358 [hep-ph].
- [17] H. Fujii, F. Gelis, and R. Venugopalan, “Quark pair production in high energy pA collisions: General features,” *Nucl.Phys.* **A780** (2006) 146–174, arXiv:hep-ph/0603099 [hep-ph].
- [18] R. Sharma and I. Vitev, “High transverse momentum quarkonium production and dissociation in heavy ion collisions,” *Phys.Rev.* **C87** no. 4, (2013) 044905, arXiv:1203.0329 [hep-ph].
- [19] F. Arleo and S. Peigné, “Heavy-quarkonium suppression in p-A collisions from parton energy loss in cold QCD matter,” *JHEP* **1303** (2013) 122, arXiv:1212.0434 [hep-ph].
- [20] P. Braun-Munzinger and J. Stachel, “(Non)thermal aspects of charmonium production and a new look at J/ψ suppression,” *Phys.Lett.* **B490** (2000) 196–202, arXiv:nucl-th/0007059 [nucl-th].
- [21] R. L. Thews, M. Schroedter, and J. Rafelski, “Enhanced J/ψ production in deconfined quark matter,” *Phys.Rev.* **C63** (2001) 054905, arXiv:hep-ph/0007323 [hep-ph].
- [22] **NA50** Collaboration, B. Alessandro *et al.*, “A new measurement of J/ψ suppression in Pb-Pb collisions at 158-GeV per nucleon,” *Eur.Phys.J.* **C39** (2005) 335–345, arXiv:hep-ex/0412036 [hep-ex].
- [23] **NA60** Collaboration, R. Arnaldi *et al.*, “ J/ψ production in indium-indium collisions at 158-GeV/nucleon,” *Phys.Rev.Lett.* **99** (2007) 132302.
- [24] **NA60** Collaboration, R. Arnaldi, “ J/ψ production in p-A and A-A collisions at fixed target experiments,” *Nucl.Phys.* **A830** (2009) 345C–352C, arXiv:0907.5004 [nucl-ex].

- [25] **PHENIX** Collaboration, A. Adare *et al.*, “ J/ψ suppression at forward rapidity in Au+Au collisions at $\sqrt{s_{NN}} = 200$ GeV,” *Phys.Rev.* **C84** (2011) 054912, arXiv:1103.6269 [nucl-ex].
- [26] **STAR** Collaboration, B. Abelev *et al.*, “ J/ψ production at high transverse momentum in p+p and Cu+Cu collisions at $\sqrt{s_{NN}} = 200$ GeV,” *Phys.Rev.* **C80** (2009) 041902, arXiv:0904.0439 [nucl-ex].
- [27] **ALICE** Collaboration, B. Abelev *et al.*, “ J/ψ suppression at forward rapidity in Pb-Pb collisions at $\sqrt{s_{NN}} = 2.76$ TeV,” *Phys.Rev.Lett.* **109** (2012) 072301, arXiv:1202.1383 [hep-ex].
- [28] **CMS** Collaboration, S. Chatrchyan *et al.*, “Suppression of non-prompt J/ψ , prompt J/ψ , and $\Upsilon(1S)$ in PbPb collisions at $\sqrt{s_{NN}} = 2.76$ TeV,” *JHEP* **1205** (2012) 063, arXiv:1201.5069 [nucl-ex].
- [29] **ATLAS** Collaboration, G. Aad *et al.*, “Measurement of the centrality dependence of J/ψ yields and observation of Z production in lead-lead collisions with the ATLAS detector at the LHC,” *Phys.Lett.* **B697** (2011) 294–312, arXiv:1012.5419 [hep-ex].
- [30] **ALICE** Collaboration, B. B. Abelev *et al.*, “Centrality, rapidity and transverse momentum dependence of J/ψ suppression in Pb-Pb collisions at $\sqrt{s_{NN}}=2.76$ TeV,” *Phys.Lett.* **B734** (2014) 314–327, arXiv:1311.0214 [nucl-ex].
- [31] **ALICE** Collaboration, B. B. Abelev *et al.*, “Inclusive, prompt and non-prompt J/ψ production at mid-rapidity in Pb-Pb collisions at $\sqrt{s_{NN}} = 2.76$ TeV,” *in preparation* .
- [32] E. Ferreira, F. Fleuret, J. Lansberg, and A. Rakotozafindrabe, “Impact of the Nuclear Modification of the Gluon Densities on J/ψ production in pPb collisions at $\sqrt{s_{NN}} = 5$ TeV,” *Phys.Rev.* **C88** no. 4, (2013) 047901, arXiv:1305.4569 [hep-ph].
- [33] J. Albacete, N. Armesto, R. Baier, G. Barnafoldi, J. Barrette, *et al.*, “Predictions for p+Pb Collisions at $\sqrt{s_{NN}} = 5$ TeV,” *Int.J.Mod.Phys.* **E22** (2013) 1330007, arXiv:1301.3395 [hep-ph].
- [34] **ALICE** Collaboration, B. B. Abelev *et al.*, “Suppression of $\psi(2S)$ production in p-Pb collisions at $\sqrt{s_{NN}} = 5.02$ TeV,” arXiv:1405.3796 [nucl-ex].
- [35] F. Arleo, R. Kolevatov, S. Peigné, and M. Rustamova, “Centrality and p_{\perp} dependence of J/ψ suppression in proton-nucleus collisions from parton energy loss,” *JHEP* **1305** (2013) 155, arXiv:1304.0901 [hep-ph].
- [36] H. Fujii and K. Watanabe, “Heavy quark pair production in high energy pA collisions: Quarkonium,” *Nucl.Phys.* **A915** (2013) 1–23, arXiv:1304.2221 [hep-ph].
- [37] **ALICE** Collaboration, K. Aamodt *et al.*, “Alignment of the ALICE Inner Tracking System with cosmic-ray tracks,” *JINST* **5** (2010) P03003, arXiv:1001.0502 [physics.ins-det].
- [38] J. Alme, Y. Andres, H. Appelshäuser, S. Bablok, N. Bialas, *et al.*, “The ALICE TPC, a large 3-dimensional tracking device with fast readout for ultra-high multiplicity events,” *Nucl.Instrum.Meth.* **A622** (2010) 316–367, arXiv:1001.1950 [physics.ins-det].
- [39] **ALICE** Collaboration, K. Aamodt *et al.*, “The ALICE experiment at the CERN LHC,” *JINST* **3** (2008) S08002.
- [40] **ALICE** Collaboration, B. Abelev *et al.*, “Measurement of the Cross Section for Electromagnetic Dissociation with Neutron Emission in Pb-Pb Collisions at $\sqrt{s_{NN}} = 2.76$ TeV,” *Phys.Rev.Lett.* **109** (2012) 252302, arXiv:1203.2436 [nucl-ex].
- [41] **ALICE** Collaboration, E. Abbas *et al.*, “Performance of the ALICE VZERO system,” *JINST* **8** (2013) P10016, arXiv:1306.3130 [nucl-ex].
- [42] **ALICE** Collaboration, B. Abelev *et al.*, “Pseudorapidity density of charged particles in p-Pb collisions at $\sqrt{s_{NN}} = 5.02$ TeV,” *Phys.Rev.Lett.* **110** (2013) 032301, arXiv:1210.3615 [nucl-ex].
- [43] **ALICE** Collaboration, B. B. Abelev *et al.*, “Measurement of visible cross sections in proton-lead

- collisions at $\sqrt{s_{NN}} = 5.02$ TeV in van der Meer scans with the ALICE detector,” *JINST* **9** no. 11, (2014) P11003, arXiv:1405.1849 [nucl-ex].
- [44] **ALICE** Collaboration, K. Aamodt *et al.*, “Rapidity and transverse momentum dependence of inclusive J/ψ production in pp collisions at $\sqrt{s} = 7$ TeV,” *Phys.Lett.* **B704** (2011) 442–455, Erratum *Phys. Lett.* **B718**(2012) 692–698, arXiv:1105.0380 [hep-ex].
- [45] J. Gaiser, *SLAC Stanford - SLAC-255 (82.REC.JUN.83)*, <http://www.slac.stanford.edu/cgi-wrap/getdoc/slac-r-255.pdf>, p.194 (1983).
- [46] R. Shahoyan, “Ph.D. Thesis,” *Instituto Superior Técnico, Lisbon, Portugal, 2001*, <http://www.cern.ch/NA50/theses/ruben.ps.gz>.
- [47] **ALICE** Collaboration, B. Abelev *et al.*, “ J/ψ polarization in pp collisions at $\sqrt{s} = 7$ TeV,” *Phys.Rev.Lett.* **108** (2012) 082001, arXiv:1111.1630 [hep-ex].
- [48] **LHCb** Collaboration, R. Aaij *et al.*, “Measurement of J/ψ production in pp collisions at $\sqrt{s} = 7$ TeV,” *Eur.Phys.J.* **C71** (2011) 1645, arXiv:1103.0423 [hep-ex].
- [49] **CMS** Collaboration, S. Chatrchyan *et al.*, “Measurement of the prompt J/ψ and $\psi(2S)$ polarizations in pp collisions at $\sqrt{s} = 7$ TeV,” *Phys.Lett.* **B727** (2013) 381–402, arXiv:1307.6070 [hep-ex].
- [50] X.-N. Wang and M. Gyulassy, “HIJING: A Monte Carlo model for multiple jet production in pp, p-A and A-A collisions,” *Phys.Rev.* **D44** (1991) 3501–3516.
- [51] R. Brun, F. Carminati, and S. Giani, “GEANT detector description and simulation tool,” *CERN-W-5013*.
- [52] L. Aphecetche *et al.*, *ALICE Internal Note ALICE-INT-2009-044*, <https://edms.cern.ch/document/1054937/1>.
- [53] **Particle Data Group** Collaboration, J. Beringer *et al.*, “Review of Particle Physics (RPP),” *Phys.Rev.* **D86** (2012) 010001.
- [54] **PHENIX** Collaboration, A. Adare *et al.*, “ J/ψ production versus transverse momentum and rapidity in p+p collisions at $\sqrt{s} = 200$ -GeV,” *Phys.Rev.Lett.* **98** (2007) 232002, arXiv:hep-ex/0611020 [hep-ex].
- [55] **CDF** Collaboration, D. Acosta *et al.*, “Measurement of the J/ψ meson and b -hadron production cross sections in $p\bar{p}$ collisions at $\sqrt{s} = 1960$ GeV,” *Phys.Rev.* **D71** (2005) 032001, arXiv:hep-ex/0412071 [hep-ex].
- [56] **ALICE** Collaboration, B. Abelev *et al.*, “Inclusive J/ψ production in pp collisions at $\sqrt{s} = 2.76$ TeV,” *Phys.Lett.* **B718** (2012) 295–306, arXiv:1203.3641 [hep-ex].
- [57] F. Bossú, Z. C. del Valle, A. de Falco, M. Gagliardi, S. Grigoryan, *et al.*, “Phenomenological interpolation of the inclusive J/ψ cross section to proton-proton collisions at 2.76 TeV and 5.5 TeV,” arXiv:1103.2394 [nucl-ex].
- [58] **LHCb** Collaboration, R. Aaij *et al.*, “Production of J/ψ and Υ mesons in pp collisions at $\sqrt{s} = 8$ TeV,” *JHEP* **1306** (2013) 064, arXiv:1304.6977 [hep-ex].
- [59] **ALICE**, **LHCb** Collaboration, ALICE and L. Collaborations, “Reference pp cross-sections for J/ψ studies in proton-lead collisions at $\sqrt{s_{NN}} = 5.02$ TeV and comparisons between ALICE and LHCb results,”.
- [60] **ALICE** Collaboration, B. B. Abelev *et al.*, “Measurement of quarkonium production at forward rapidity in pp collisions at $\sqrt{s} = 7$ TeV,” *Eur.Phys.J.* **C74** no. 8, (2014) 2974, arXiv:1403.3648 [nucl-ex].
- [61] **ALICE** Collaboration, B. Abelev *et al.*, “Measurement of prompt J/ψ and beauty hadron production cross sections at mid-rapidity in pp collisions at $\sqrt{s} = 7$ TeV,” *JHEP* **1211** (2012) 065, arXiv:1205.5880 [hep-ex].
- [62] R. Vogt, “Shadowing and absorption effects on J/ψ production in dA collisions,” *Phys.Rev.* **C71**

- (2005) 054902, arXiv:hep-ph/0411378 [hep-ph].
- [63] R. Vogt, “Cold Nuclear Matter Effects on J/ψ and Υ Production at the LHC,” *Phys.Rev.* **C81** (2010) 044903, arXiv:1003.3497 [hep-ph].
- [64] E. Ferreiro, F. Fleuret, J. Lansberg, and A. Rakotozafindrabe, “Cold nuclear matter effects on J/ψ production: intrinsic and extrinsic transverse momentum effects,” *Phys.Lett.* **B680** (2009) 50–55, arXiv:0809.4684 [hep-ph].

A The ALICE Collaboration

J. Adam³⁹, D. Adamová⁸², M.M. Aggarwal⁸⁶, G. Aglieri Rinella³⁶, M. Agnello¹¹⁰, N. Agrawal⁴⁷, Z. Ahammed¹³⁰, I. Ahmed¹⁶, S.U. Ahn⁶⁷, I. Aimo^{93,110}, S. Aiola¹³⁵, M. Ajaz¹⁶, A. Akindinov⁵⁷, S.N. Alam¹³⁰, D. Aleksandrov⁹⁹, B. Alessandro¹¹⁰, D. Alexandre¹⁰¹, R. Alfaro Molina⁶³, A. Alici^{104,12}, A. Alkin³, J. Alme³⁷, T. Alt⁴², S. Altinpinar¹⁸, I. Altsybeev¹²⁹, C. Alves Garcia Prado¹¹⁸, C. Andrei⁷⁷, A. Andronic⁹⁶, V. Anguelov⁹², J. Anielski⁵³, T. Antičić⁹⁷, F. Antinori¹⁰⁷, P. Antonioli¹⁰⁴, L. Aphecetche¹¹², H. Appelshäuser⁵², S. Arcelli²⁸, N. Armesto¹⁷, R. Arnaldi¹¹⁰, T. Aronsson¹³⁵, I.C. Arsene²², M. Arslanodk⁵², A. Augustinus³⁶, R. Averbeck⁹⁶, M.D. Azmi¹⁹, M. Bach⁴², A. Badalà¹⁰⁶, Y.W. Baek⁴³, S. Bagnasco¹¹⁰, R. Bailhache⁵², R. Bala⁸⁹, A. Baldisseri¹⁵, F. Baltasar Dos Santos Pedrosa³⁶, R.C. Baral⁶⁰, A.M. Barbaño¹¹⁰, R. Barbera²⁹, F. Barile³³, G.G. Barnaföldi¹³⁴, L.S. Barnby¹⁰¹, V. Barret⁶⁹, P. Bartalini⁷, J. Bartke¹¹⁵, E. Bartsch⁵², M. Basile²⁸, N. Bastid⁶⁹, S. Basu¹³⁰, B. Bathen⁵³, G. Batigne¹¹², A. Batista Camejo⁶⁹, B. Batyunya⁶⁵, P.C. Batzing²², I.G. Bearden⁷⁹, H. Beck⁵², C. Bedda¹¹⁰, N.K. Behera⁴⁷, I. Belikov⁵⁴, F. Bellini²⁸, H. Bello Martinez², R. Bellwied¹²⁰, R. Belmont¹³³, E. Belmont-Moreno⁶³, V. Belyaev⁷⁵, G. Bencedi¹³⁴, S. Beole²⁷, I. Berceau⁷⁷, A. Bercuci⁷⁷, Y. Berdnikov⁸⁴, D. Berenyi¹³⁴, R.A. Bertens⁵⁶, D. Berzano^{36,27}, L. Betev³⁶, A. Bhasin⁸⁹, I.R. Bhat⁸⁹, A.K. Bhati⁸⁶, B. Bhattacharjee⁴⁴, J. Bhom¹²⁶, L. Bianchi^{27,120}, N. Bianchi⁷¹, C. Bianchin^{133,56}, J. Bielčik³⁹, J. Bielčiková⁸², A. Bilandzic⁷⁹, S. Biswas⁷⁸, S. Bjelogrić⁵⁶, F. Blanco¹⁰, D. Blau⁹⁹, C. Blume⁵², F. Bock^{73,92}, A. Bogdanov⁷⁵, H. Bøggild⁷⁹, L. Boldizsár¹³⁴, M. Bombara⁴⁰, J. Book⁵², H. Borel¹⁵, A. Borissov⁹⁵, M. Borri⁸¹, F. Bossu⁶⁴, M. Botje⁸⁰, E. Botta²⁷, S. Böttger⁵¹, P. Braun-Munzinger⁹⁶, M. Bregant¹¹⁸, T. Breitner⁵¹, T.A. Broker⁵², T.A. Browning⁹⁴, M. Broz³⁹, E.J. Brucken⁴⁵, E. Bruna¹¹⁰, G.E. Bruno³³, D. Budnikov⁹⁸, H. Buesching⁵², S. Bufalino^{36,110}, P. Buncic³⁶, O. Busch⁹², Z. Buthelezi⁶⁴, J.T. Buxton²⁰, D. Caffarri^{36,30}, X. Cai⁷, H. Caines¹³⁵, L. Calero Diaz⁷¹, A. Caliva⁵⁶, E. Calvo Villar¹⁰², P. Camerini²⁶, F. Carena³⁶, W. Carena³⁶, J. Castillo Castellanos¹⁵, A.J. Castro¹²³, E.A.R. Casula²⁵, C. Cavicchioli³⁶, C. Ceballos Sanchez⁹, J. Cepila³⁹, P. Cerello¹¹⁰, B. Chang¹²¹, S. Chapeland³⁶, M. Chartier¹²², J.L. Charvet¹⁵, S. Chattopadhyay¹³⁰, S. Chattopadhyay¹⁰⁰, V. Chelnokov³, M. Cherney⁸⁵, C. Cheshkov¹²⁸, B. Cheynis¹²⁸, V. Chibante Barroso³⁶, D.D. Chinellato¹¹⁹, P. Chochula³⁶, K. Choi⁹⁵, M. Chojnacki⁷⁹, S. Choudhury¹³⁰, P. Christakoglou⁸⁰, C.H. Christensen⁷⁹, P. Christiansen³⁴, T. Chujo¹²⁶, S.U. Chung⁹⁵, C. Cicalo¹⁰⁵, L. Cifarelli^{12,28}, F. Cindolo¹⁰⁴, J. Cleymans⁸⁸, F. Colamaria³³, D. Colella³³, A. Collu²⁵, M. Colocci²⁸, G. Conesa Balbastre⁷⁰, Z. Conesa del Valle⁵⁰, M.E. Connors¹³⁵, J.G. Contreras^{39,11}, T.M. Cormier⁸³, Y. Corrales Morales²⁷, I. Cortés Maldonado², P. Cortese³², M.R. Cosentino¹¹⁸, F. Costa³⁶, P. Crochet⁶⁹, R. Cruz Albino¹¹, E. Cuautle⁶², L. Cunqueiro³⁶, T. Dahms⁹¹, A. Dainese¹⁰⁷, A. Danu⁶¹, D. Das¹⁰⁰, I. Das^{100,50}, S. Das⁴, A. Dash¹¹⁹, S. Dash⁴⁷, S. De¹¹⁸, A. De Caro^{31,12}, G. de Cataldo¹⁰³, J. de Cuveland⁴², A. De Falco²⁵, D. De Gruttola^{12,31}, N. De Marco¹¹⁰, S. De Pasquale³¹, A. Deisting^{96,92}, A. Deloff⁷⁶, E. Dénes¹³⁴, G. D'Erasmus³³, D. Di Bari³³, A. Di Mauro³⁶, P. Di Nezza⁷¹, M.A. Diaz Corchero¹⁰, T. Dietel⁸⁸, P. Dillenseger⁵², R. Divià³⁶, Ø. Djuvsland¹⁸, A. Dobrin^{56,80}, T. Dobrowolski^{76,i}, D. Domenicis Gimenez¹¹⁸, B. Dönigus⁵², O. Dordic²², A.K. Dubey¹³⁰, A. Dubla⁵⁶, L. Ducroux¹²⁸, P. Dupieux⁶⁹, R.J. Ehlers¹³⁵, D. Elia¹⁰³, H. Engel⁵¹, B. Erasmus^{112,36}, F. Erhardt¹²⁷, D. Eschweiler⁴², B. Espagnon⁵⁰, M. Estienne¹¹², S. Esumi¹²⁶, J. Eum⁹⁵, D. Evans¹⁰¹, S. Evdokimov¹¹¹, G. Eyyubova³⁹, L. Fabbietti⁹¹, D. Fabris¹⁰⁷, J. Faivre⁷⁰, A. Fantoni⁷¹, M. Fasel⁷³, L. Feldkamp⁵³, D. Felea⁶¹, A. Feliciello¹¹⁰, G. Feofilov¹²⁹, J. Ferencei⁸², A. Fernández Téllez², E.G. Ferreira¹⁷, A. Ferretti²⁷, A. Festanti³⁰, J. Figiel¹¹⁵, M.A.S. Figueredo¹²², S. Filchagin⁹⁸, D. Finogeev⁵⁵, F.M. Fionda¹⁰³, E.M. Fiore³³, M. Floris³⁶, S. Foertsch⁶⁴, P. Foka⁹⁶, S. Fokin⁹⁹, E. Fragiaco¹⁰⁹, A. Francescon^{36,30}, U. Frankendorf⁹⁶, U. Fuchs³⁶, C. Furget⁷⁰, A. Furs⁵⁵, M. Fusco Girard³¹, J.J. Gaardhøje⁷⁹, M. Gagliardi²⁷, A.M. Gago¹⁰², M. Gallio²⁷, D.R. Gangadharan⁷³, P. Ganoti⁸⁷, C. Gao⁷, C. Garabatos⁹⁶, E. Garcia-Solis¹³, C. Gargiulo³⁶, P. Gasik⁹¹, M. Germain¹¹², A. Gheata³⁶, M. Gheata^{61,36}, P. Ghosh¹³⁰, S.K. Ghosh⁴, P. Gianotti⁷¹, P. Giubellino³⁶, P. Giubilato³⁰, E. Gladysz-Dziadus¹¹⁵, P. Glässel⁹², A. Gomez Ramirez⁵¹, P. González-Zamora¹⁰, S. Gorbunov⁴², L. Görlich¹¹⁵, S. Gotovac¹¹⁴, V. Grabski⁶³, L.K. Graczykowski¹³², A. Grelli⁵⁶, A. Grigoras³⁶, C. Grigoras³⁶, V. Grigoriev⁷⁵, A. Grigoryan¹, S. Grigoryan⁶⁵, B. Grinyov³, N. Grion¹⁰⁹, J.F. Grosse-Oetringhaus³⁶, J.-Y. Grossiord¹²⁸, R. Grosso³⁶, F. Guber⁵⁵, R. Guernane⁷⁰, B. Guerzoni²⁸, K. Gulbrandsen⁷⁹, H. Gulkanyan¹, T. Gunji¹²⁵, A. Gupta⁸⁹, R. Gupta⁸⁹, R. Haake⁵³, Ø. Haaland¹⁸, C. Hadjidakis⁵⁰, M. Haiduc⁶¹, H. Hamagaki¹²⁵, G. Hamar¹³⁴, L.D. Hanratty¹⁰¹, A. Hansen⁷⁹, J.W. Harris¹³⁵, H. Hartmann⁴², A. Harton¹³, D. Hatzifotiadou¹⁰⁴, S. Hayashi¹²⁵, S.T. Heckel⁵², M. Heide⁵³, H. Helstrup³⁷, A. Herghelegiu⁷⁷, G. Herrera Corral¹¹, B.A. Hess³⁵, K.F. Hetland³⁷, T.E. Hilden⁴⁵, H. Hillemanns³⁶, B. Hippolyte⁵⁴, P. Hristov³⁶, M. Huang¹⁸, T.J. Humanic²⁰, N. Hussain⁴⁴, T. Hussain¹⁹, D. Hutter⁴², D.S. Hwang²¹, R. Ilkaev⁹⁸, I. Ilkiv⁷⁶, M. Inaba¹²⁶, C. Ionita³⁶, M. Ippolitov^{75,99}, M. Irfan¹⁹, M. Ivanov⁹⁶, V. Ivanov⁸⁴, V. Izucheev¹¹¹, P.M. Jacobs⁷³, C. Jahnke¹¹⁸, H.J. Jang⁶⁷, M.A. Janik¹³², P.H.S.Y. Jayarathna¹²⁰, C. Jena³⁰, S. Jena¹²⁰, R.T. Jimenez Bustamante⁶²,

P.G. Jones¹⁰¹, H. Jung⁴³, A. Jusko¹⁰¹, P. Kalinak⁵⁸, A. Kalweit³⁶, J. Kamin⁵², J.H. Kang¹³⁶, V. Kaplin⁷⁵, S. Kar¹³⁰, A. Karasu Uysal⁶⁸, O. Karavichev⁵⁵, T. Karavicheva⁵⁵, E. Karpechev⁵⁵, U. Kebschull⁵¹, R. Keidel¹³⁷, D.L.D. Keijdener⁵⁶, M. Keil³⁶, K.H. Khan¹⁶, M.M. Khan¹⁹, P. Khan¹⁰⁰, S.A. Khan¹³⁰, A. Khanzadeev⁸⁴, Y. Kharlov¹¹¹, B. Kileng³⁷, B. Kim¹³⁶, D.W. Kim^{43,67}, D.J. Kim¹²¹, H. Kim¹³⁶, J.S. Kim⁴³, M. Kim⁴³, M. Kim¹³⁶, S. Kim²¹, T. Kim¹³⁶, S. Kirsch⁴², I. Kisel⁴², S. Kiselev⁵⁷, A. Kisiel¹³², G. Kiss¹³⁴, J.L. Klay⁶, C. Klein⁵², J. Klein⁹², C. Klein-Bösing⁵³, A. Kluge³⁶, M.L. Knichel⁹², A.G. Knospe¹¹⁶, T. Kobayashi¹²⁶, C. Kobdaj¹¹³, M. Kofarago³⁶, M.K. Köhler⁹⁶, T. Kollegger^{96,42}, A. Kolojvari¹²⁹, V. Kondratiev¹²⁹, N. Kondratyeva⁷⁵, E. Kondratyuk¹¹¹, A. Konevskikh⁵⁵, C. Kouzinopoulos³⁶, O. Kovalenko⁷⁶, V. Kovalenko¹²⁹, M. Kowalski^{36,115}, S. Kox⁷⁰, G. Koyithatta Meethalevedu⁴⁷, J. Kral¹²¹, I. Králik⁵⁸, A. Kravčáková⁴⁰, M. Krelina³⁹, M. Kretz⁴², M. Krivda^{58,101}, F. Krizek⁸², E. Kryshen³⁶, M. Krzewicki^{42,96}, A.M. Kubera²⁰, V. Kučera⁸², T. Kugathasan³⁶, C. Kuhn⁵⁴, P.G. Kuijser⁸⁰, I. Kulakov⁴², J. Kumar⁴⁷, L. Kumar^{78,86}, P. Kurashvili⁷⁶, A. Kurepin⁵⁵, A.B. Kurepin⁵⁵, A. Kuryakin⁹⁸, S. Kushpil⁸², M.J. Kweon⁴⁹, Y. Kwon¹³⁶, S.L. La Pointe¹¹⁰, P. La Rocca²⁹, C. Lagana Fernandes¹¹⁸, I. Lakomov^{50,36}, R. Langoy⁴¹, C. Lara⁵¹, A. Lardeux¹⁵, A. Lattuca²⁷, E. Laudi³⁶, R. Lea²⁶, L. Leardini⁹², G.R. Lee¹⁰¹, S. Lee¹³⁶, I. Legrand³⁶, R.C. Lemmon⁸¹, V. Lenti¹⁰³, E. Leogrande⁵⁶, I. León Monzón¹¹⁷, M. Leoncino²⁷, P. Lévai¹³⁴, S. Li^{7,69}, X. Li¹⁴, J. Lien⁴¹, R. Lietava¹⁰¹, S. Lindal²², V. Lindenstruth⁴², C. Lippmann⁹⁶, M.A. Lisa²⁰, H.M. Ljunggren³⁴, D.F. Lodato⁵⁶, P.I. Loenne¹⁸, V.R. Loggins¹³³, V. Loginov⁷⁵, C. Loizides⁷³, X. Lopez⁶⁹, E. López Torres⁹, A. Lowe¹³⁴, X.-G. Lu⁹², P. Luettig⁵², M. Lunardon³⁰, G. Luparello^{26,56}, P.H.F.N.D. Luz¹¹⁸, A. Maevskaya⁵⁵, M. Mager³⁶, S. Mahajan⁸⁹, S.M. Mahmood²², A. Maire⁵⁴, R.D. Majka¹³⁵, M. Malaev⁸⁴, I. Maldonado Cervantes⁶², L. Malinina⁶⁵, D. Mal'Kevich⁵⁷, P. Malzacher⁹⁶, A. Mamonov⁹⁸, L. Manceau¹¹⁰, V. Manko⁹⁹, F. Manso⁶⁹, V. Manzari^{36,103}, M. Marchisone²⁷, J. Mareš⁵⁹, G.V. Margagliotti²⁶, A. Margotti¹⁰⁴, J. Margutti⁵⁶, A. Marín⁹⁶, C. Markert¹¹⁶, M. Marquard⁵², N.A. Martin⁹⁶, J. Martin Blanco¹¹², P. Martinengo³⁶, M.I. Martínez², G. Martínez García¹¹², M. Martinez Pedreira³⁶, Y. Martynov³, A. Mas¹¹⁸, S. Masciocchi⁹⁶, M. Maserà²⁷, A. Masoni¹⁰⁵, L. Massacrier¹¹², A. Mastroserio³³, H. Masui¹²⁶, A. Matyja¹¹⁵, C. Mayer¹¹⁵, J. Mazer¹²³, M.A. Mazzoni¹⁰⁸, D. McDonald¹²⁰, F. Meddi²⁴, A. Menchaca-Rocha⁶³, E. Meninno³¹, J. Mercado Pérez⁹², M. Meres³⁸, Y. Miake¹²⁶, M.M. Mieskolainen⁴⁵, K. Mikhaylov^{57,65}, L. Milano³⁶, J. Milosevic^{22,131}, L.M. Minervini^{23,103}, A. Mischke⁵⁶, A.N. Mishra⁴⁸, D. Miśkowiec⁹⁶, J. Mitra¹³⁰, C.M. Mitu⁶¹, N. Mohammadi⁵⁶, B. Mohanty^{130,78}, L. Molnar⁵⁴, L. Montaño Zetina¹¹, E. Montes¹⁰, M. Morando³⁰, D.A. Moreira De Godoy¹¹², S. Moretto³⁰, A. Morreale¹¹², A. Morsch³⁶, V. Muccifora⁷¹, E. Mudnic¹¹⁴, D. Mühlheim⁵³, S. Muhuri¹³⁰, M. Mukherjee¹³⁰, H. Müller³⁶, J.D. Mulligan¹³⁵, M.G. Munhoz¹¹⁸, S. Murray⁶⁴, L. Musa³⁶, J. Musinsky⁵⁸, B.K. Nandi⁴⁷, R. Nania¹⁰⁴, E. Nappi¹⁰³, M.U. Naru¹⁶, C. Nattrass¹²³, K. Nayak⁷⁸, T.K. Nayak¹³⁰, S. Nazarenko⁹⁸, A. Nedosekin⁵⁷, L. Nellen⁶², F. Ng¹²⁰, M. Nicassio⁹⁶, M. Niculescu^{61,36}, J. Niedziela³⁶, B.S. Nielsen⁷⁹, S. Nikolaev⁹⁹, S. Nikulin⁹⁹, V. Nikulin⁸⁴, F. Noferini^{104,12}, P. Nomokonov⁶⁵, G. Nooren⁵⁶, J. Norman¹²², A. Nyanin⁹⁹, J. Nystrand¹⁸, H. Oeschler⁹², S. Oh¹³⁵, S.K. Oh⁶⁶, A. Ohlson³⁶, A. Okatan⁶⁸, T. Okubo⁴⁶, L. Olah¹³⁴, J. Oleniacz¹³², A.C. Oliveira Da Silva¹¹⁸, M.H. Oliver¹³⁵, J. Onderwaater⁹⁶, C. Oppedisano¹¹⁰, A. Ortiz Velasquez⁶², A. Oskarsson³⁴, J. Otwinowski^{96,115}, K. Oyama⁹², M. Ozdemir⁵², Y. Pachmayer⁹², P. Pagano³¹, G. Paic⁶², C. Pajares¹⁷, S.K. Pal¹³⁰, J. Pan¹³³, D. Pant⁴⁷, V. Papikyan¹, G.S. Pappalardo¹⁰⁶, P. Pareek⁴⁸, W.J. Park⁹⁶, S. Parmar⁸⁶, A. Passfeld⁵³, V. Paticchio¹⁰³, B. Paul¹⁰⁰, T. Pawlak¹³², T. Peitzmann⁵⁶, H. Pereira Da Costa¹⁵, E. Pereira De Oliveira Filho¹¹⁸, D. Peresunko^{75,99}, C.E. Pérez Lara⁸⁰, V. Peskov⁵², Y. Pestov⁵, V. Petráček³⁹, V. Petrov¹¹¹, M. Petrovici⁷⁷, C. Petta²⁹, S. Piano¹⁰⁹, M. Pikna³⁸, P. Pillot¹¹², O. Pinazza^{104,36}, L. Pinsky¹²⁰, D.B. Piyarathna¹²⁰, M. Płoskoń⁷³, M. Planinic¹²⁷, J. Pluta¹³², S. Pochybova¹³⁴, P.L.M. Podesta-Lerma¹¹⁷, M.G. Poghosyan⁸⁵, B. Polichtchouk¹¹¹, N. Poljak¹²⁷, W. Poonsawat¹¹³, A. Pop⁷⁷, S. Porteboeuf-Houssais⁶⁹, J. Porter⁷³, J. Pospisil⁸², S.K. Prasad⁴, R. Preghenella^{104,36}, F. Prino¹¹⁰, C.A. Pruneau¹³³, I. Pshenichnov⁵⁵, M. Puccio¹¹⁰, G. Puddu²⁵, P. Pujahari¹³³, V. Punin⁹⁸, J. Putschke¹³³, H. Qvigstad²², A. Rachevski¹⁰⁹, S. Raha⁴, S. Rajput⁸⁹, J. Rak¹²¹, A. Rakotozafindrabe¹⁵, L. Ramello³², R. Raniwala⁹⁰, S. Raniwala⁹⁰, S.S. Räsänen⁴⁵, B.T. Rascanu⁵², D. Rathee⁸⁶, K.F. Read¹²³, J.S. Real⁷⁰, K. Redlich⁷⁶, R.J. Reed¹³³, A. Rehman¹⁸, P. Reichelt⁵², M. Reicher⁵⁶, F. Reidt^{36,92}, X. Ren⁷, R. Renfordt⁵², A.R. Reolon⁷¹, A. Reshetin⁵⁵, F. Rettig⁴², J.-P. Revol¹², K. Reygers⁹², V. Riabov⁸⁴, R.A. Ricci⁷², T. Richert³⁴, M. Richter²², P. Riedler³⁶, W. Riegler³⁶, F. Riggi²⁹, C. Ristea⁶¹, A. Rivetti¹¹⁰, E. Rocco⁵⁶, M. Rodríguez Cahuantzi^{2,11}, A. Rodríguez Manso⁸⁰, K. Røed²², E. Rogochaya⁶⁵, D. Rohr⁴², D. Röhrich¹⁸, R. Romita¹²², F. Ronchetti⁷¹, L. Ronflette¹¹², P. Rosnet⁶⁹, A. Rossi³⁶, F. Roukoutakis⁸⁷, A. Roy⁴⁸, C. Roy⁵⁴, P. Roy¹⁰⁰, A.J. Rubio Montero¹⁰, R. Rui²⁶, R. Russo²⁷, E. Ryabinkin⁹⁹, Y. Ryabov⁸⁴, A. Rybicki¹¹⁵, S. Sadovsky¹¹¹, K. Šafařík³⁶, B. Sahlmüller⁵², P. Sahoo⁴⁸, R. Sahoo⁴⁸, S. Sahoo⁶⁰, P.K. Sahu⁶⁰, J. Saini¹³⁰, S. Sakai⁷¹, M.A. Saleh¹³³, C.A. Salgado¹⁷, J. Salzwedel²⁰, S. Sambyal⁸⁹, V. Samsonov⁸⁴, X. Sanchez Castro⁵⁴, L. Šándor⁵⁸, A. Sandoval⁶³, M. Sano¹²⁶, G. Santagati²⁹, D. Sarkar¹³⁰, E. Scapparone¹⁰⁴, F. Scarlassara³⁰,

R.P. Scharenberg⁹⁴, C. Schiaua⁷⁷, R. Schicker⁹², C. Schmidt⁹⁶, H.R. Schmidt³⁵, S. Schuchmann⁵², J. Schukraft³⁶, M. Schulc³⁹, T. Schuster¹³⁵, Y. Schutz^{112,36}, K. Schwarz⁹⁶, K. Schweda⁹⁶, G. Scioli²⁸, E. Scomparin¹¹⁰, R. Scott¹²³, K.S. Seeder¹¹⁸, J.E. Seger⁸⁵, Y. Sekiguchi¹²⁵, I. Selyuzhenkov⁹⁶, K. Senosi⁶⁴, J. Seo^{66,95}, E. Serradilla^{10,63}, A. Sevcenco⁶¹, A. Shabanov⁵⁵, A. Shabetai¹¹², O. Shadura³, R. Shahoyan³⁶, A. Shangaraev¹¹¹, A. Sharma⁸⁹, N. Sharma^{60,123}, K. Shigaki⁴⁶, K. Shtejer^{9,27}, Y. Sibiriak⁹⁹, S. Siddhanta¹⁰⁵, K.M. Sielewicz³⁶, T. Siemiarczuk⁷⁶, D. Silvermyr^{83,34}, C. Silvestre⁷⁰, G. Simatovic¹²⁷, G. Simonetti³⁶, R. Singaraju¹³⁰, R. Singh⁷⁸, S. Singha^{78,130}, V. Singhal¹³⁰, B.C. Sinha¹³⁰, T. Sinha¹⁰⁰, B. Sitar³⁸, M. Sitta³², T.B. Skaali²², M. Slupecki¹²¹, N. Smirnov¹³⁵, R.J.M. Snellings⁵⁶, T.W. Snellman¹²¹, C. Sogaard³⁴, R. Soltz⁷⁴, J. Song⁹⁵, M. Song¹³⁶, Z. Song⁷, F. Soramel³⁰, S. Sorensen¹²³, M. Spacek³⁹, E. Spiriti⁷¹, I. Sputowska¹¹⁵, M. Spyropoulou-Stassinaki⁸⁷, B.K. Srivastava⁹⁴, J. Stachel⁹², I. Stan⁶¹, G. Stefanek⁷⁶, M. Steinpreis²⁰, E. Stenlund³⁴, G. Steyn⁶⁴, J.H. Stiller⁹², D. Stocco¹¹², P. Strmen³⁸, A.A.P. Suaide¹¹⁸, T. Sugitate⁴⁶, C. Suire⁵⁰, M. Suleymanov¹⁶, R. Sultanov⁵⁷, M. Šumbera⁸², T.J.M. Symons⁷³, A. Szabo³⁸, A. Szanto de Toledo¹¹⁸, I. Szarka³⁸, A. Szczepankiewicz³⁶, M. Szymanski¹³², J. Takahashi¹¹⁹, N. Tanaka¹²⁶, M.A. Tangaro³³, J.D. Tapia Takaki⁵⁰, A. Tarantola Peloni⁵², M. Tariq¹⁹, M.G. Tarzila⁷⁷, A. Tauro³⁶, G. Tejada Muñoz², A. Telesca³⁶, K. Terasaki¹²⁵, C. Terrevoli^{30,25}, B. Teyssier¹²⁸, J. Thäder^{96,73}, D. Thomas¹¹⁶, R. Tieulent¹²⁸, A.R. Timmins¹²⁰, A. Toia⁵², S. Trogolo¹¹⁰, V. Trubnikov³, W.H. Trzaska¹²¹, T. Tsuji¹²⁵, A. Tumkin⁹⁸, R. Turrisi¹⁰⁷, T.S. Tveter²², K. Ullaland¹⁸, A. Uras¹²⁸, G.L. Usai²⁵, A. Utrobicic¹²⁷, M. Vajzer⁸², M. Vala⁵⁸, L. Valencia Palomo⁶⁹, S. Vallerio²⁷, J. Van Der Maarel⁵⁶, J.W. Van Hoorne³⁶, M. van Leeuwen⁵⁶, T. Vanat⁸², P. Vande Vyvre³⁶, D. Varga¹³⁴, A. Vargas², M. Vargyas¹²¹, R. Varma⁴⁷, M. Vasileiou⁸⁷, A. Vasiliev⁹⁹, A. Vauthier⁷⁰, V. Vechemin¹²⁹, A.M. Veen⁵⁶, M. Veldhoen⁵⁶, A. Velure¹⁸, M. Venaruzzo⁷², E. Vercellin²⁷, S. Vergara Limón², R. Vernet⁸, M. Verweij¹³³, L. Vickovic¹¹⁴, G. Viesti^{30,i}, J. Viinikainen¹²¹, Z. Vilakazi¹²⁴, O. Villalobos Baillie¹⁰¹, A. Vinogradov⁹⁹, L. Vinogradov¹²⁹, Y. Vinogradov⁹⁸, T. Virgili³¹, V. Vislavicius³⁴, Y.P. Viyogi¹³⁰, A. Vodopyanov⁶⁵, M.A. Völkl⁹², K. Voloshin⁵⁷, S.A. Voloshin¹³³, G. Volpe^{36,134}, B. von Haller³⁶, I. Vorobyev⁹¹, D. Vranic^{96,36}, J. Vrláková⁴⁰, B. Vulpescu⁶⁹, A. Vyushin⁹⁸, B. Wagner¹⁸, J. Wagner⁹⁶, H. Wang⁵⁶, M. Wang^{7,112}, Y. Wang⁹², D. Watanabe¹²⁶, M. Weber³⁶, S.G. Weber⁹⁶, J.P. Wessels⁵³, U. Westerhoff⁵³, J. Wiechula³⁵, J. Wikne²², M. Wilde⁵³, G. Wilk⁷⁶, J. Wilkinson⁹², M.C.S. Williams¹⁰⁴, B. Windelband⁹², M. Winn⁹², C.G. Yaldo¹³³, Y. Yamaguchi¹²⁵, H. Yang⁵⁶, P. Yang⁷, S. Yano⁴⁶, S. Yasnopolskiy⁹⁹, Z. Yin⁷, H. Yokoyama¹²⁶, I.-K. Yoo⁹⁵, V. Yurchenko³, I. Yushmanov⁹⁹, A. Zaborowska¹³², V. Zaccolo⁷⁹, A. Zaman¹⁶, C. Zampolli¹⁰⁴, H.J.C. Zanoli¹¹⁸, S. Zaporozhets⁶⁵, A. Zarochentsev¹²⁹, P. Závada⁵⁹, N. Zaviyalov⁹⁸, H. Zbroszczyk¹³², I.S. Zgura⁶¹, M. Zhalov⁸⁴, H. Zhang⁷, X. Zhang⁷³, Y. Zhang⁷, C. Zhao²², N. Zhigareva⁵⁷, D. Zhou⁷, Y. Zhou⁵⁶, Z. Zhou¹⁸, H. Zhu⁷, J. Zhu^{7,112}, X. Zhu⁷, A. Zichichi^{12,28}, A. Zimmermann⁹², M.B. Zimmermann^{53,36}, G. Zinovjev³, M. Zyzak⁴²

Affiliation notes

ⁱ Deceased

Collaboration Institutes

- ¹ A.I. Alikhanyan National Science Laboratory (Yerevan Physics Institute) Foundation, Yerevan, Armenia
- ² Benemérita Universidad Autónoma de Puebla, Puebla, Mexico
- ³ Bogolyubov Institute for Theoretical Physics, Kiev, Ukraine
- ⁴ Bose Institute, Department of Physics and Centre for Astroparticle Physics and Space Science (CAPSS), Kolkata, India
- ⁵ Budker Institute for Nuclear Physics, Novosibirsk, Russia
- ⁶ California Polytechnic State University, San Luis Obispo, California, United States
- ⁷ Central China Normal University, Wuhan, China
- ⁸ Centre de Calcul de l'IN2P3, Villeurbanne, France
- ⁹ Centro de Aplicaciones Tecnológicas y Desarrollo Nuclear (CEADEN), Havana, Cuba
- ¹⁰ Centro de Investigaciones Energéticas Medioambientales y Tecnológicas (CIEMAT), Madrid, Spain
- ¹¹ Centro de Investigación y de Estudios Avanzados (CINVESTAV), Mexico City and Mérida, Mexico
- ¹² Centro Fermi - Museo Storico della Fisica e Centro Studi e Ricerche "Enrico Fermi", Rome, Italy
- ¹³ Chicago State University, Chicago, Illinois, USA
- ¹⁴ China Institute of Atomic Energy, Beijing, China
- ¹⁵ Commissariat à l'Energie Atomique, IRFU, Saclay, France
- ¹⁶ COMSATS Institute of Information Technology (CIIT), Islamabad, Pakistan

- 17 Departamento de Física de Partículas and IGFAE, Universidad de Santiago de Compostela, Santiago de Compostela, Spain
- 18 Department of Physics and Technology, University of Bergen, Bergen, Norway
- 19 Department of Physics, Aligarh Muslim University, Aligarh, India
- 20 Department of Physics, Ohio State University, Columbus, Ohio, United States
- 21 Department of Physics, Sejong University, Seoul, South Korea
- 22 Department of Physics, University of Oslo, Oslo, Norway
- 23 Dipartimento di Elettrotecnica ed Elettronica del Politecnico, Bari, Italy
- 24 Dipartimento di Fisica dell'Università 'La Sapienza' and Sezione INFN Rome, Italy
- 25 Dipartimento di Fisica dell'Università and Sezione INFN, Cagliari, Italy
- 26 Dipartimento di Fisica dell'Università and Sezione INFN, Trieste, Italy
- 27 Dipartimento di Fisica dell'Università and Sezione INFN, Turin, Italy
- 28 Dipartimento di Fisica e Astronomia dell'Università and Sezione INFN, Bologna, Italy
- 29 Dipartimento di Fisica e Astronomia dell'Università and Sezione INFN, Catania, Italy
- 30 Dipartimento di Fisica e Astronomia dell'Università and Sezione INFN, Padova, Italy
- 31 Dipartimento di Fisica 'E.R. Caianiello' dell'Università and Gruppo Collegato INFN, Salerno, Italy
- 32 Dipartimento di Scienze e Innovazione Tecnologica dell'Università del Piemonte Orientale and Gruppo Collegato INFN, Alessandria, Italy
- 33 Dipartimento Interateneo di Fisica 'M. Merlin' and Sezione INFN, Bari, Italy
- 34 Division of Experimental High Energy Physics, University of Lund, Lund, Sweden
- 35 Eberhard Karls Universität Tübingen, Tübingen, Germany
- 36 European Organization for Nuclear Research (CERN), Geneva, Switzerland
- 37 Faculty of Engineering, Bergen University College, Bergen, Norway
- 38 Faculty of Mathematics, Physics and Informatics, Comenius University, Bratislava, Slovakia
- 39 Faculty of Nuclear Sciences and Physical Engineering, Czech Technical University in Prague, Prague, Czech Republic
- 40 Faculty of Science, P.J. Šafárik University, Košice, Slovakia
- 41 Faculty of Technology, Buskerud and Vestfold University College, Vestfold, Norway
- 42 Frankfurt Institute for Advanced Studies, Johann Wolfgang Goethe-Universität Frankfurt, Frankfurt, Germany
- 43 Gangneung-Wonju National University, Gangneung, South Korea
- 44 Gauhati University, Department of Physics, Guwahati, India
- 45 Helsinki Institute of Physics (HIP), Helsinki, Finland
- 46 Hiroshima University, Hiroshima, Japan
- 47 Indian Institute of Technology Bombay (IIT), Mumbai, India
- 48 Indian Institute of Technology Indore, Indore (IITI), India
- 49 Inha University, Incheon, South Korea
- 50 Institut de Physique Nucléaire d'Orsay (IPNO), Université Paris-Sud, CNRS-IN2P3, Orsay, France
- 51 Institut für Informatik, Johann Wolfgang Goethe-Universität Frankfurt, Frankfurt, Germany
- 52 Institut für Kernphysik, Johann Wolfgang Goethe-Universität Frankfurt, Frankfurt, Germany
- 53 Institut für Kernphysik, Westfälische Wilhelms-Universität Münster, Münster, Germany
- 54 Institut Pluridisciplinaire Hubert Curien (IPHC), Université de Strasbourg, CNRS-IN2P3, Strasbourg, France
- 55 Institute for Nuclear Research, Academy of Sciences, Moscow, Russia
- 56 Institute for Subatomic Physics of Utrecht University, Utrecht, Netherlands
- 57 Institute for Theoretical and Experimental Physics, Moscow, Russia
- 58 Institute of Experimental Physics, Slovak Academy of Sciences, Košice, Slovakia
- 59 Institute of Physics, Academy of Sciences of the Czech Republic, Prague, Czech Republic
- 60 Institute of Physics, Bhubaneswar, India
- 61 Institute of Space Science (ISS), Bucharest, Romania
- 62 Instituto de Ciencias Nucleares, Universidad Nacional Autónoma de México, Mexico City, Mexico
- 63 Instituto de Física, Universidad Nacional Autónoma de México, Mexico City, Mexico
- 64 iThemba LABS, National Research Foundation, Somerset West, South Africa
- 65 Joint Institute for Nuclear Research (JINR), Dubna, Russia
- 66 Konkuk University, Seoul, South Korea
- 67 Korea Institute of Science and Technology Information, Daejeon, South Korea

- 68 KTO Karatay University, Konya, Turkey
- 69 Laboratoire de Physique Corpusculaire (LPC), Clermont Université, Université Blaise Pascal, CNRS-IN2P3, Clermont-Ferrand, France
- 70 Laboratoire de Physique Subatomique et de Cosmologie, Université Grenoble-Alpes, CNRS-IN2P3, Grenoble, France
- 71 Laboratori Nazionali di Frascati, INFN, Frascati, Italy
- 72 Laboratori Nazionali di Legnaro, INFN, Legnaro, Italy
- 73 Lawrence Berkeley National Laboratory, Berkeley, California, United States
- 74 Lawrence Livermore National Laboratory, Livermore, California, United States
- 75 Moscow Engineering Physics Institute, Moscow, Russia
- 76 National Centre for Nuclear Studies, Warsaw, Poland
- 77 National Institute for Physics and Nuclear Engineering, Bucharest, Romania
- 78 National Institute of Science Education and Research, Bhubaneswar, India
- 79 Niels Bohr Institute, University of Copenhagen, Copenhagen, Denmark
- 80 Nikhef, National Institute for Subatomic Physics, Amsterdam, Netherlands
- 81 Nuclear Physics Group, STFC Daresbury Laboratory, Daresbury, United Kingdom
- 82 Nuclear Physics Institute, Academy of Sciences of the Czech Republic, Řež u Prahy, Czech Republic
- 83 Oak Ridge National Laboratory, Oak Ridge, Tennessee, United States
- 84 Petersburg Nuclear Physics Institute, Gatchina, Russia
- 85 Physics Department, Creighton University, Omaha, Nebraska, United States
- 86 Physics Department, Panjab University, Chandigarh, India
- 87 Physics Department, University of Athens, Athens, Greece
- 88 Physics Department, University of Cape Town, Cape Town, South Africa
- 89 Physics Department, University of Jammu, Jammu, India
- 90 Physics Department, University of Rajasthan, Jaipur, India
- 91 Physik Department, Technische Universität München, Munich, Germany
- 92 Physikalisches Institut, Ruprecht-Karls-Universität Heidelberg, Heidelberg, Germany
- 93 Politecnico di Torino, Turin, Italy
- 94 Purdue University, West Lafayette, Indiana, United States
- 95 Pusan National University, Pusan, South Korea
- 96 Research Division and ExtreMe Matter Institute EMMI, GSI Helmholtzzentrum für Schwerionenforschung, Darmstadt, Germany
- 97 Rudjer Bošković Institute, Zagreb, Croatia
- 98 Russian Federal Nuclear Center (VNIIEF), Sarov, Russia
- 99 Russian Research Centre Kurchatov Institute, Moscow, Russia
- 100 Saha Institute of Nuclear Physics, Kolkata, India
- 101 School of Physics and Astronomy, University of Birmingham, Birmingham, United Kingdom
- 102 Sección Física, Departamento de Ciencias, Pontificia Universidad Católica del Perú, Lima, Peru
- 103 Sezione INFN, Bari, Italy
- 104 Sezione INFN, Bologna, Italy
- 105 Sezione INFN, Cagliari, Italy
- 106 Sezione INFN, Catania, Italy
- 107 Sezione INFN, Padova, Italy
- 108 Sezione INFN, Rome, Italy
- 109 Sezione INFN, Trieste, Italy
- 110 Sezione INFN, Turin, Italy
- 111 SSC IHEP of NRC Kurchatov institute, Protvino, Russia
- 112 SUBATECH, Ecole des Mines de Nantes, Université de Nantes, CNRS-IN2P3, Nantes, France
- 113 Suranaree University of Technology, Nakhon Ratchasima, Thailand
- 114 Technical University of Split FESB, Split, Croatia
- 115 The Henryk Niewodniczanski Institute of Nuclear Physics, Polish Academy of Sciences, Cracow, Poland
- 116 The University of Texas at Austin, Physics Department, Austin, Texas, USA
- 117 Universidad Autónoma de Sinaloa, Culiacán, Mexico
- 118 Universidade de São Paulo (USP), São Paulo, Brazil
- 119 Universidade Estadual de Campinas (UNICAMP), Campinas, Brazil
- 120 University of Houston, Houston, Texas, United States

- 121 University of Jyväskylä, Jyväskylä, Finland
- 122 University of Liverpool, Liverpool, United Kingdom
- 123 University of Tennessee, Knoxville, Tennessee, United States
- 124 University of the Witwatersrand, Johannesburg, South Africa
- 125 University of Tokyo, Tokyo, Japan
- 126 University of Tsukuba, Tsukuba, Japan
- 127 University of Zagreb, Zagreb, Croatia
- 128 Université de Lyon, Université Lyon 1, CNRS/IN2P3, IPN-Lyon, Villeurbanne, France
- 129 V. Fock Institute for Physics, St. Petersburg State University, St. Petersburg, Russia
- 130 Variable Energy Cyclotron Centre, Kolkata, India
- 131 Vinča Institute of Nuclear Sciences, Belgrade, Serbia
- 132 Warsaw University of Technology, Warsaw, Poland
- 133 Wayne State University, Detroit, Michigan, United States
- 134 Wigner Research Centre for Physics, Hungarian Academy of Sciences, Budapest, Hungary
- 135 Yale University, New Haven, Connecticut, United States
- 136 Yonsei University, Seoul, South Korea
- 137 Zentrum für Technologietransfer und Telekommunikation (ZTT), Fachhochschule Worms, Worms, Germany